



Perfect, broadband, and sub-wavelength absorption with asymmetric absorbers: Realization for duct acoustics with 3D printed porous resonators

Jean Boulvert^{a,b,c,*}, Thomas Humbert^a, Vicente Romero-García^a, Gwénaél Gabard^a, Edith Roland Fotsing^b, Annie Ross^b, Jacky Mardjono^c, Jean-Philippe Groby^a

^a Laboratoire d'Acoustique de l'Université du Mans, LAUM - UMR CNRS 6613, Le Mans Université, Avenue Olivier Messiaen, 72085 Le Mans Cedex 9, France

^b Laboratoire d'Analyse Vibratoire et Acoustique, LAVA, Mechanical engineering, Polytechnique Montréal, Montréal, Québec, Canada

^c Safran Aircraft Engines, Villaroche, Rond Point René Ravaud - Réau, 77550 Moisy-Cramayel Cedex, France

ARTICLE INFO

Keywords:

Duct acoustics
Perfect absorption
Asymmetric absorber
Sub-wavelength
Additive manufacturing
Porous material

ABSTRACT

This article explores, theoretically and experimentally, asymmetric absorbers made of detuned and folded quarter wavelength resonators filled with air or porous materials. When used as acoustic lining in ducts, their thickness can be sub-wavelength and they can be designed for perfect absorption in broad target frequency bandwidth. The considered filling porous material can be easily 3D printed and is formed of a structured micro-lattice with variable lattice constant, allowing precise control of its acoustic properties. The underlying physics of asymmetric absorbers is discussed through a simplified analysis by means of the transfer matrix method. The behavior of the porous absorbers is also predicted by a mode-matching technique accounting for the possible couplings between the resonators. An absorber made of folded quarter-wavelength resonators is optimized, 3D printed and experimentally tested. The experimental results are in good agreement with the theory and show a mean absorption coefficient of 99% over almost an octave and below the quarter-wavelength frequency corresponding to the height of the absorber.

1. Introduction

A large variety of engineering applications involve duct noise problems such as car exhaust systems, mechanical housing ventilation systems, or aircraft engines. The width of the duct varies from less than a centimeter to meters. The noise frequency range depends on the main acoustic source, e.g., a car engine operating at a certain rotation speed, and of secondary sources such as the interaction of an air flux with the duct walls. Acoustic treatments can reduce noise emissions while allowing free air flow: mufflers are designed to reduce the transmission of sound waves, [1], anechoic terminations to avoid backward reflection at the end of a duct [2], and absorbers to simultaneously reduce the transmission while avoiding reflection, i.e., to absorb sound waves [3]. In this work, we focus on absorbers targeting perfect absorption, i.e., no reflection and no transmission, and more specifically on asymmetric absorbers, whose losses are carefully controlled by porous materials, that are flush mounted to the walls of a straight duct whose width is of the order of centimeters.

* Corresponding author at: Laboratoire d'Acoustique de l'Université du Mans, LAUM - UMR CNRS 6613, Le Mans Université, Avenue Olivier Messiaen, 72085 Le Mans Cedex 9, France.

E-mail address: jean.boulvert@univ-lemans.fr (J. Boulvert).

<https://doi.org/10.1016/j.jsv.2021.116687>

Received 27 May 2021; Received in revised form 3 December 2021; Accepted 7 December 2021

Available online 30 December 2021

0022-460X/© 2021 Elsevier Ltd. All rights reserved.

Homogeneous open-cell porous materials are widely used as acoustic treatments. Their behavior is well described by propagation models and their efficiency to operate as broadband acoustic absorbing panels has long been theoretically, numerically and experimentally demonstrated. They are sometimes used to control noise propagation through ducts, e.g., in porous car mufflers [1]. Nevertheless, when perfect absorption is targeted in ducted propagation, porous materials are often set aside so far due to physical reasons, mostly in favor of Helmholtz resonators (HRs) [3–13]. Using conventional porous materials in an optimization problem is frequently not fully satisfactory because of the lack of flexibility in the choice of their properties and their low efficiency in the sub-wavelength regime. Yet, recent advances in additive manufacturing now makes it possible to easily design and manufacture porous materials having controlled pore shapes and dimensions, which allows to fully control their intrinsic acoustic behavior [14–18]. This way, the optimization of 3D printed acoustic treatments comprising porous materials is not limited to a catalog of existing materials.

Targeting perfect absorption in a duct or waveguide requires either an asymmetric absorber [3,10] or the use of degenerate resonators with symmetric (monopolar) and antisymmetric (dipolar) resonances [8–10]. So far, asymmetric absorbers achieving very high absorption over a broad target frequency bandwidth are either compact but make use of a very narrow waveguide (≤ 1 mm high) [5] or make use of a waveguide of the order of centimeters wide but are not compact, i.e., the resonators forming the absorber are spaced by several centimeters [11]. In this work, we explore the absorption capabilities of porous asymmetric absorbers because 3D printing allows to easily control porous materials intrinsic properties. The studied porous absorbers are composed of locally reacting, detuned and possibly folded quarter-wavelength resonators (QWRs) filled with porous materials with controlled pore size or air. The absorbers are flush mounted to the walls of a straight waveguide of a few centimeters wide and of rectangular cross-section.

The objective of this work is twofold: (1) to show that compact absorbers can exhibit a very high absorption over broad target frequency bandwidths when flush mounted on waveguides of the order of centimeters wide and (2) to show that porous absorbers used in ducted problems can be efficient at frequencies below the quarter-wavelength frequency corresponding to the height of the absorbers.

In a first stage, the physical principles and limitations of asymmetric absorbers are described through a transfer matrix method (TMM) analysis. This analysis leads to simple analytical conditions on the surface impedance to obtain perfect absorption. This analysis also provides an expression for the minimal absorber length (dimension in the direction of propagation of the incident wave) combining the frequency and the size of the duct. This expression highlights that the length of the absorber can easily be lower than a quarter of the targeted wavelength λ in air and that the real challenge is to consider a waveguide with a cross-section greatly larger than the area of the resonators surface connected to the waveguide. In a second stage, the absorbers are optimized by making use of a model that considers the potential coupling between the resonators for physically realistic waveguide configurations, demonstrating that an absorption coefficient of mean value close to unity over a broad target frequency bandwidth can be achieved in a duct using porous resonators in their sub-wavelength regime as acoustic lining. More specifically, a porous absorber with a height of less than $\lambda/4$, is designed by using folded QWRs to lower the resonance frequencies of the resonators without modifying their height. This absorber exhibits experimentally a 99% absorption over almost one octave.

The article is organized as follows: first, the porous asymmetric absorbers are introduced in Section 2. The considered porous medium, its manufacturing and its acoustic behavior are presented, along with the geometry of the porous absorbers including that of folded porous resonators. Then, the analytical and numerical modeling procedures of waveguides lined by porous absorbers are described in Section 3. In Section 4, the analysis of the asymmetric absorbers is performed using TMM predictions. The conditions to reach perfect absorption by means of asymmetric sound absorbers are derived and expressed in terms of the resonators surface impedance. In Section 5, porous absorbers are numerically optimized for realistic conditions. In addition, an example of a sub-wavelength absorber optimized for perfect absorption over a broad target frequency range is manufactured and tested experimentally, showing a good correlation between measured and predicted absorption.

2. Porous asymmetric absorbers

This section introduces the asymmetric porous absorbers studied in this work and their constitutive elements: QWRs filled with a porous medium or by air.

2.1. Asymmetric absorber lining a duct of constant cross section

Perfect absorption in a duct propagation problem can be obtained when the propagation symmetry is broken [3], when degenerated resonators are used [9], or when symmetry inversion frequency is tuned [19]. The simplest system is thus an asymmetric absorber [3] that is composed of at least two different resonators placed at a finite distance from each other along the duct axial direction. In this work, we focus on ducts of the order of centimeters wide and of constant cross section. The absorbers are flush mounted to the walls of the duct walls, so as not to change its cross section. This feature is chosen to limit the perturbations of the air flow in the duct. The absorbers line part, or all, of the walls of the duct. Usually, the resonators composing the duct absorbers are HRs. We focus here on QWRs filled either with air or with a porous medium.

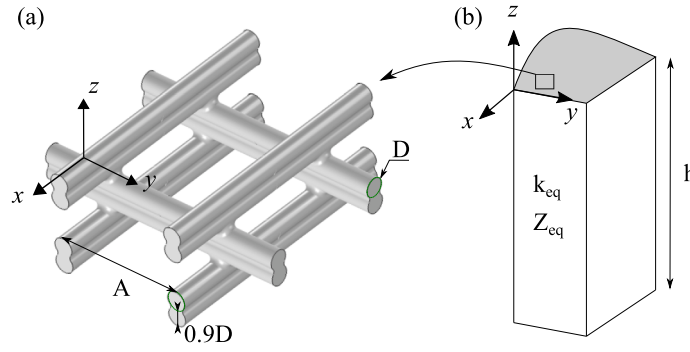


Fig. 1. QWR filled with porous medium. (a) Diagram of the porous material microstructure named micro-lattice. The normal direction of the medium is z and is aligned to the normal direction of the QWRs. (b) QWR of arbitrary cross-section and height h .

2.2. Porous medium

The porous medium filling the QWRs is a micro-lattice. The optimizations are performed considering this specific medium for efficiency purposes, but other media such as stochastic foams could have also been used. An idealized representation of the micro-lattice is depicted in Fig. 1(a). This medium is fibrous, structured, periodic, quasi-isotropic and can be 3D printed. It is composed of a superposition of layers of parallel rods, each layer being orthogonal to the previous one. Each rod is a combination of two filaments of diameter D fused with one another in the vertical direction. The vertical, (O, z) , distance between the center of two successive filaments is $0.9D$. The horizontal distance between the center of two rods, i.e., the lattice constant, is named A . Both D and A can be tuned.

The optimized absorbers are made by additive manufacturing and more specifically by Fused Deposition Modeling (FDM) technique. The slicer software and printer used in this work are *Simplify3D* and *RAISE3D Pro2*, respectively. The extruded material is polylactic acid (PLA). A $200\ \mu\text{m}$ diameter nozzle is used to produce the micro-lattice. The manufacturing parameter that controls the lattice constant, A , is named “infill factor”, $IF = 100/(AD)$, and is then inversely proportional to A .

2.3. QWRs filled with an anisotropic porous medium or air

The QWRs of the proposed absorbers are either filled with air or with the micro-lattice. This allows us to control the amount of losses introduced in each QWR.

2.3.1. Equivalent fluid modeling

To account for the acoustic losses occurring inside the QWRs, they are filled with equivalent fluids that are defined by an equivalent density ρ_{eq} and an equivalent bulk modulus K_{eq} , both being complex and frequency dependent. K_{eq} is a scalar and ρ_{eq} is a scalar if the filling medium is isotropic (e.g. air) or is a matrix if the filling medium is anisotropic (e.g. the quasi-isotropic micro-lattice).

The losses in a QWR filled with air arise from the viscous and thermal boundary layers along its walls. These losses are accounted for by the Stinson’s model [20] considering an equivalent hydraulic radius to account for any type of QWR section. By contrast, the losses in a QWR filled with a porous medium arise mainly from the porous medium itself. Its corresponding equivalent fluid is described here by the well-known Johnson–Champoux–Allard–Lafarge (JCAL) model [21,22]. It provides a frequency-dependent description of ρ_{eq} and K_{eq} by means of parameters depending on the porous medium micro-structure and called JCAL parameters. These are the porosity, ϕ , the tortuosity α_∞ , the viscous and thermal characteristic lengths, Λ and Λ' and the viscous and thermal static permeabilities q_0 and q'_0 . As can be seen in Fig. C.13 of the Appendix, ϕ , Λ , Λ' , q_0 and q'_0 decrease and α_∞ increases when the IF increases which indicates that the intrinsic losses and the resistivity of the micro-lattice increases when the IF increases (i.e., as the lattice constant decreases).

During the porous absorber optimization, IF can take values comprised between 3% and 70%. In practice, it is only possible to manufacture integer percentage values of IF. As the micro-lattice fills QWRs of small lateral dimensions, for very low IF values, the lattice constant is close to the lateral size of the QWRs and the micro-lattice can no longer be considered as a homogeneous porous medium. For this reason the micro-lattice is replaced by air when the IF values are lower than 5%.

2.3.2. Surface impedance

Expression of the surface impedance. The QWRs composing the porous absorbers are forced to be of sufficiently small lateral dimensions compared to the acoustic wavelength to be considered as locally reacting resonators which behavior can be expressed through a surface impedance simplifying the waveguide propagation equations.

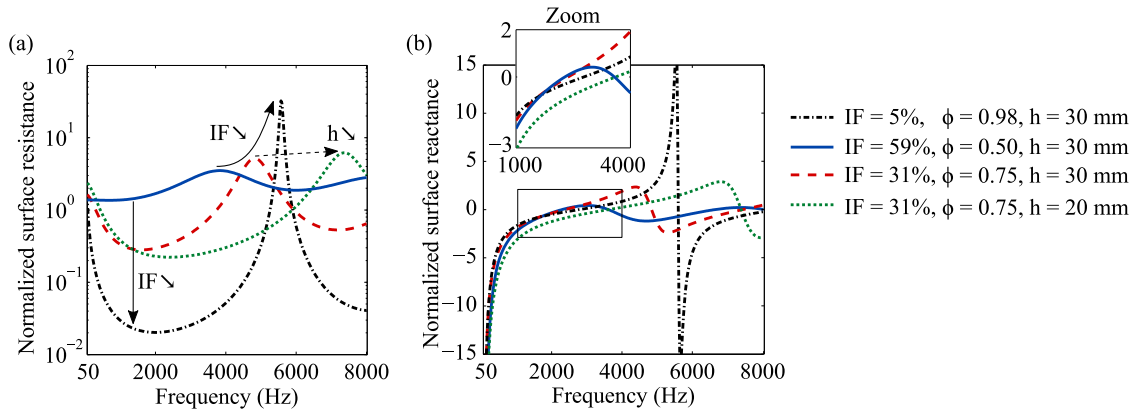


Fig. 2. (color online) Normalized surface impedance of QWRs filled with homogeneous micro-lattices. The height of the QWRs is 30 mm or 20 mm. The diameter of the manufacturing nozzle is $200\mu\text{m}$ and the IF is equal to 5%, 31% or 59%, corresponding to a porosity of 0.98, 0.75 or 0.50, respectively. (a) Normalized surface resistance. (b) Normalized surface reactance.

With an implicit time dependence $e^{i\omega t}$, and only accounting for normal propagation into the QWRs (locally reacting hypothesis), the surface impedance of a straight QWR filled with an homogeneous equivalent fluid is [22]

$$Z_s = -iZ_{eq} \cot(k_{eq}h), \tag{1}$$

where h is the height of the QWR, see Fig. 1(b). k_{eq} and Z_{eq} are the equivalent fluid wave number and characteristic impedance, respectively, in the normal direction z . k_{eq} and Z_{eq} can be derived from ρ_{eq} and K_{eq} [23].

Propagation models that do not account for high order modes in the main waveguide, such as the TMM, require a length correction h_δ at the opening of the QWRs. A purely imaginary impedance is then added to Z_s and the QWR corrected surface impedance is

$$Z_s^c = Z_s + iZ_0k_0h_\delta, \tag{2}$$

in which $k_0 = \omega/c_0$ is the wave number of air in the waveguide and Z_0 is the characteristic impedance of the air in the waveguide. An expression of h_δ is in Ref. [24] for QWRs sections much smaller than $1/k_0$.

Discussion about the surface impedance. If a QWR is filled with air and its intrinsic losses are neglected, the surface impedance reduces to $Z_s = -iZ_0 \cot(k_0h)$. The only parameter of the QWR that controls Z_s is thus its height h . The surface resistance is zero for all frequencies and the surface reactance vanishes at the resonance frequencies of the QWR. Adding the length correction h_δ does not change the resistance and slightly shifts the null reactance frequencies. In practice, the intrinsic losses of a QWR are never exactly zero. As a consequence, its surface resistance is never exactly zero but its surface reactance still vanishes at the resonance frequencies.

If a QWR is filled with a micro-lattice, Z_s still depends on the QWR height h but also on the micro-lattice properties which vary with the filaments diameter and the lattice constant. In practice, the lattice constant and the height of the QWR can be easily tuned. For a given QWR height and 3D printer nozzle diameter, increasing the micro-lattice IF decreases the porous material lattice constant and thus increases its porosity and decreases its resistivity. This results in an increase of the quality factor of the porous QWR modes. Indeed, as depicted in Fig. 2, the peak of surface resistance and of surface reactance at the second quarter-wavelength frequency are sharper for lower IF values and the resistance is lower before and after the resistance peak. Moreover, the lower the IF, the higher the resonance frequency. Note that the surface resistance is never zero and its minimal value is obtained with the lowest authorized value of IF. In addition, as expected from Eq. (1), for a given IF (i.e., a given set of k_{eq} and Z_{eq}) decreasing the height h of the QWR increases the second quarter-wavelength frequency of the QWR and modifies its surface resistance and reactance. In particular, before the second quarter-wavelength frequency, the surface reactance is reduced (see zoom in Fig. 2(b)).

Therefore, the surface impedance of a QWR filled with a homogeneous micro-lattice can be tuned by varying the IF of the micro-lattice and the QWR height. However, this tuning is limited by the fact that the surface impedance has peaks and valleys over the frequency range due to the QWR resonances and anti-resonances. Because of the intrinsic losses, a null surface resistance cannot be attained. The range of realizable impedance will determine how close the absorption coefficient of the absorber is to one. Around the resonance frequency of the QWR, where the QWR has the most impact on the absorber behavior, its surface reactance is mostly controlled by the QWR height and is approximately equal to $-Z_0 \cot(k_0h)$. The minimum (resp. maximum) reachable surface resistance is obtained by minimizing (resp. maximizing) the QWR intrinsic losses. A very permeable (resp. resistive) porous material will lead to low (resp. high) losses. The lowest losses are obtained when filling the QWR with air.

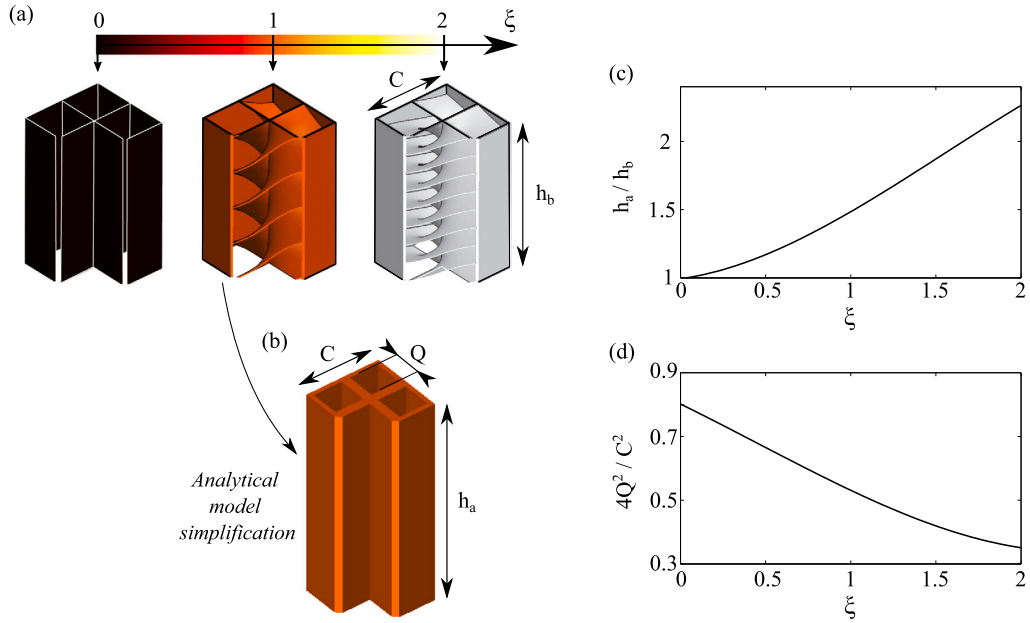


Fig. 3. (a) Geometry of the structure of the folded QWRs with respect to ξ . (b) Simplified geometry of the $\xi = 1$ folded QWR. (c) Normalized height of the simplified folded QWRs in function of ξ . (d) Normalized section of the simplified folded QWRs in function of ξ .

2.3.3. Sub-wavelength folded QWRs

The term “sub-wavelength” usually indicates that an acoustic treatment of height h reaches perfect absorption at normal incidence when rigidly backed for a frequency corresponding to a wavelength in air λ that is much larger than $4h$. In practice, it is used to differentiate conventional porous treatments having a weak sub-wavelength behavior, i.e., that cannot reach perfect absorption at normal incidence with $h \ll \lambda/4$, from other types of resonator based structures or resonant structures having a strong sub-wavelength behavior, such as treatments based on HRs. Treatments made of porous materials can also achieve sub-wavelength absorption, for instance by incorporating resonant inclusions [25–27], optimizing a gradient of properties through their thickness [28–30] or folding their structure [31–33]. To retain the essence of the term “sub-wavelength”, we suggest using it for ducted propagation to qualify an acoustic liner whose height is much smaller than $\lambda/4$.

To reach the sub-wavelength regime, we introduce folded QWRs. The interest of folding the QWRs is that their acoustic effective height h_a is then larger than the bulk QWRs height h_b . The sub-wavelength regime can then be reached since $h_b < h_a \approx \lambda/4$ while still filling the QWRs by simple homogeneous porous materials or air. Various folding strategies have been proposed in the literature, in particular for aerospace applications [34,35]. The QWRs can be folded in a L- or U-shape or helically folded. The helically folded QWRs presented in Fig. 3(a) are selected. Unlike L- and U-shape QWRs, the volume occupied by helically folded QWRs is not affected by the folding as these QWRs roll-up under themselves. Then, the optimization of a treatment made of a collection of helically folded QWRs is simple as it does not require topology optimization. These helically folded QWRs have been used in Ref. [33] to design a metaporous surface exhibiting broadband and sub-wavelength absorption at normal incidence. We now use them to design a sub-wavelength duct absorber optimized in a particular configuration in Section 5.3. The parameters governing the surface impedance of the helically folded QWRs are the number of revolutions ξ of their governing helix over h_b and the IF of their filling micro-lattices (if not replaced by air). The acoustic effective height and section of the helically folded QWRs is obtained through the comparison of numerical and analytical computations [33]. A ξ -folded QWR of height h_b and section C^2 is considered. First, the geometry of the QWR is simplified into an unfolded QWR of section C^2 made of a quartet of straight tubes of height h_a and section Q^2 as shown in Fig. 3(b). Both the folded QWR and the simplified unfolded QWR are filled with an arbitrary equivalent fluid. Then, the reflection coefficient at normal incidence of the folded QWR is computed numerically. Finally, the h_a and Q parameters are selected so that the reflection coefficient of the simplified QWR computed analytically matches the numerically calculated impedance of the folded QWR as closely as possible. The analytical reflection coefficient at normal incidence of the unfolded QWR is given by

$$R_{QWR} = \frac{\frac{C}{4Q^2} Z_s^c - Z_0}{\frac{C}{4Q^2} Z_s^c + Z_0}, \quad (3)$$

with Z_0 being the characteristic impedance of the air and Z_s^c the corrected surface impedance of the straight tubes, Eq. (2). The variations of h_a and $4Q^2$ in function of ξ are presented in Fig. 3(c, d).

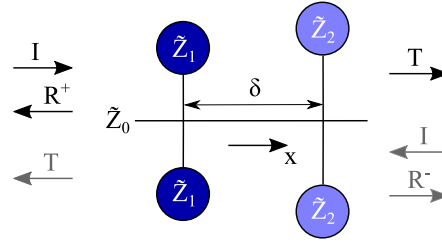


Fig. 4. Schematic representation of a 1D asymmetric absorber composed of two different groups of localized resonators separated by a distance δ . Each group is composed of two resonators. The sound wave propagates in the x direction.

3. Waveguide modeling

The acoustic behavior of a flush mounted asymmetric absorber is described by its transmission coefficient $T(f)$, its reflection coefficient defined for incident waves coming from upstream $R^+(f)$ and its reflection coefficient defined for incident waves coming from downstream $R^-(f)$. The absorption coefficient of the absorber is $\alpha^\pm(f) = 1 - |R^\pm(f)|^2 - |T(f)|^2$ and has a maximal value of 1 when the absorption is perfect, i.e., when there is no transmission and no reflection for a given incident wave direction.

This section introduces three methods to predict the acoustic behavior of asymmetric absorbers and to optimize them. The amplitude of the sound waves is low enough to consider linear propagation and there is no air flow in the waveguide.

The dimensions of the waveguide cross section are greater than or equal to 1 cm, and the optimization target frequency is always greater than 1 kHz. Then, the visco-thermal losses along the rigid walls of the waveguide are much smaller than those introduced by the designed absorbers. Moreover, they are uncoupled from the losses of the loaded resonators. This way, the predicted losses only arise from the absorbers.

3.1. Transfer matrix method

The Transfer Matrix Method (TMM) provides an approximate description of the acoustic behavior of a waveguide lined by an absorber [36]. The absorbers are formed of point resonators (i.e., with no axial extent) and plane waves are assumed to propagate along the waveguide. The possible evanescent coupling between the resonators is therefore neglected. While the TMM provides a 1D model that does not account for all the complexity of the problem at hand, it still captures the key features. This method is thus useful to derive fundamental design rules for the asymmetric absorber.

The problem considered by the TMM is outlined in Fig. 4: point resonators are connected to a propagation line representing the waveguide. The waveguide has a characteristic impedance $\tilde{Z}_0 = Z_0/S_w$ with Z_0 being the impedance of air with no losses (the losses are neglected in the waveguide) and S_w the cross-sectional area of the waveguide. Each point resonator i is modeled by the surface impedance $\tilde{Z}_i = Z_i^c/S_i$ where Z_i^c is the surface impedance of the resonator (including a length correction) and S_i is the area of the resonator surface connected to the waveguide. As the model is one-dimensional, the respective areas S_w and S_i allow to represent the correct fluxes. Appendix A provides the complete details about the formulation of the TMM model.

3.2. Realistic waveguide models accounting for possible evanescent coupling

In this section, two more realistic models are presented to predict the absorption achieved by the porous asymmetric absorbers. These models are three-dimensional and include high-order duct modes. The possible couplings between resonators are therefore accounted for.

3.2.1. Finite element method

A finite element method (FEM) model of the lined waveguide is designed with COMSOL Multiphysics® and used for validation purposes. The QWRs are filled with an equivalent fluid and the waveguide is filled with air. The losses in the system only arise from the equivalent fluids. Fig. 5(a) provides a schematic representation of this model for a waveguide lined with two straight QWRs filled with equivalent fluids. The main equation solved by the FEM model is the generalized Helmholtz equation in the fluids (air or equivalent fluid),

$$\frac{\omega^2}{K} p + \text{div}(\rho^{-1} \text{grad} p) = 0, \tag{4}$$

where ρ^{-1} and K are the inverse of the density matrix and the bulk modulus of the fluid, respectively, both being complex and frequency dependent. Impervious walls are accounted by zero-flux boundary condition

$$\text{grad} p \cdot \mathbf{n} = 0, \tag{5}$$

where \mathbf{n} is the normal vector to the walls.

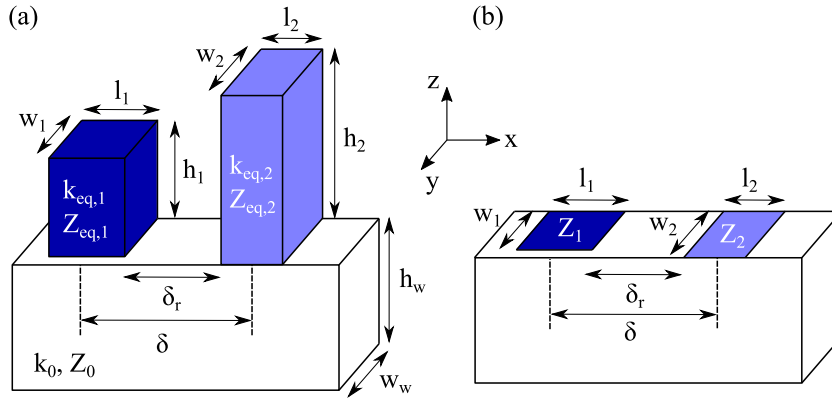


Fig. 5. Diagram of a waveguide of rectangular section lined by two QWRs filled with equivalent fluids. (a) FEM representation. (b) MMT representation.

The R^\pm and T coefficients of the absorber can be easily retrieved from the FEM simulations [37]. It involves projecting the pressure fields onto the modal basis of the rigid waveguide to obtain the modal amplitudes of the forward and backward waves and then computing R^\pm and T . Below the first cut-off frequency of the waveguide, the reflection and transmission coefficients of the absorber can be directly computed by the same technique as with a 4-microphone impedance tube (see ISO 10534-2:1998).

3.2.2. Mode matching

The mode matching technique (MMT) described by Bi et al. [38] for cylindrical waveguides is adapted here to rectangular section waveguides.

The MMT considers a waveguide of constant section with impedance boundary conditions on the walls, see Fig. 5(b). Unlike the FEM model, the full geometry of the QWRs is not directly represented as the resonators are replaced by their effective surface impedance. Rigid walls correspond to an infinite surface impedance. The surface impedance is piecewise continuous along the axial direction x and can be continuous or continuous by part in the transverse directions. In each duct section, the acoustic fields are decomposed onto the modal basis of the hard-wall waveguide. Pressure and axial velocity are matched on the axial interfaces between two duct sections with different wall impedances. Since high-order duct modes are included, frequencies above the cut-off frequency of the waveguide can be considered. Note that the modeling technique does not require any length correction at the opening of the resonators because the coupling is operated via the high-order modes of the waveguides that are accounted for. See Appendix B for more details on this MMT model.

Unlike the TMM, the MMT does not allow to write simple expressions of optimal impedances but it considers the potential coupling between the resonators while delivering faster computation times than the FEM model. For this reason, the MMT is used to predict the behavior of the absorbers during their optimization.

4. Conditions for perfect absorption in asymmetric absorbers

In this section, the TMM model is used to derive conditions to achieve perfect absorption in waveguides with asymmetric absorbers. These conditions will be exploited in Section 5 to optimize asymmetric absorbers composed of QWRs but they are general enough to be applied to any types of resonators that can be considered as point resonators as a first approximation. The present analysis focuses on maximizing α^+ , i.e., minimizing $|R^+|^2 + |T|^2$. This problem is twofold since one has to suppress both the transmission and the reflection at the incident side.

4.1. Perfect absorption at a single frequency

4.1.1. Perfect absorption conditions

Analytical expression of the perfect absorption conditions. We start by considering a simple problem: an absorber made of two different point resonators of impedance \bar{Z}_1 and \bar{Z}_2 , respectively, and separated by a distance $\delta > 0$. This distance must be non-zero to produce an asymmetric absorber as shown in Fig. 4. Each resonator can be replicated and thus replaced by a group of $N \geq 1$ identical resonators located at the same axial position, for instance on multiple (N) walls lined by the same acoustic treatment.

The absorber transmission and reflection coefficients are

$$T = \frac{2\beta_1\beta_2e^{-ik_0\delta}}{2\beta_1\beta_2 + \beta_1 + \beta_2 + i\sin(k_0\delta)e^{-ik_0\delta}}, \quad (6)$$

$$R^+ = -\frac{\beta_1e^{-2ik_0\delta} + \beta_2 + i\sin(k_0\delta)e^{-ik_0\delta}}{2\beta_1\beta_2 + \beta_1 + \beta_2 + i\sin(k_0\delta)e^{-ik_0\delta}}, \quad (7)$$

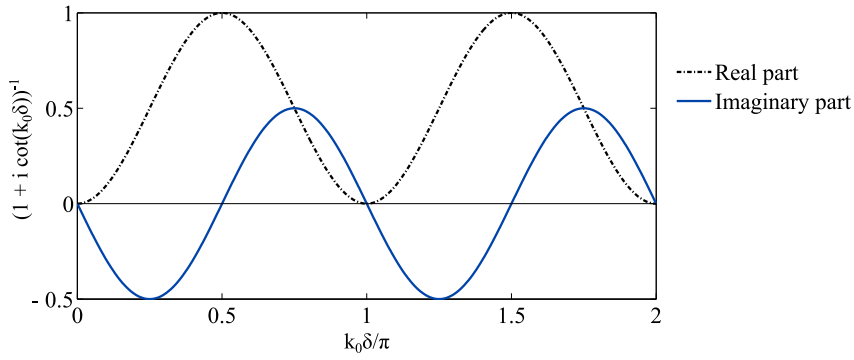


Fig. 6. Real part (dash-dot line) and imaginary part (solid line) of the right-hand side of Eq. (12) with respect to non dimensional distance between resonator groups.

$$R^- = -\frac{\beta_1 + \beta_2 e^{-2ik_0\delta} + i \sin(k_0\delta) e^{-ik_0\delta}}{2\beta_1\beta_2 + \beta_1 + \beta_2 + i \sin(k_0\delta) e^{-ik_0\delta}}, \quad (8)$$

with $\beta_1(f) = \tilde{Z}_1(f)/(N\tilde{Z}_0)$ and $\beta_2 = \tilde{Z}_2(f)/(N\tilde{Z}_0)$.

Due to the reciprocity of the system composed of the waveguide lined by the absorber, the expression for T is symmetric with respect to β_1 and β_2 , i.e., the transmission coefficient of the absorber does not depend on the incident wave direction or on the ordering of the resonator groups: $T(\beta_1, \beta_2) = T(\beta_2, \beta_1)$. Either the resonator group 1 or group 2 can be used to cancel the transmission. Here, the resonator group 2 is chosen to cancel T . To get zero transmission at a given frequency f , this second group should be designed such that

$$\beta_2 = \frac{\tilde{Z}_2(f)}{N\tilde{Z}_0} = 0 \quad \Leftrightarrow \quad Z_2^c(f) = 0. \quad (9)$$

In a less stringent form, a quasi no-transmission condition can be written as

$$\beta_2 = \frac{\tilde{Z}_2(f)}{N\tilde{Z}_0} \ll 1 \quad \Leftrightarrow \quad \frac{Z_2^c(f)}{Z_0} \ll \frac{NS_2}{S_w}. \quad (10)$$

Assuming that the resonator group 2 cancels the transmission at a given frequency f , the reflection coefficients of the absorber at that same frequency can be simplified in

$$R^+(f) = -\frac{\beta_1 e^{-ik_0\delta} + i \sin(k_0\delta)}{\beta_1 e^{+ik_0\delta} + i \sin(k_0\delta)}, \quad R^-(f) = -1, \quad \text{when } \beta_2(f) = 0. \quad (11)$$

On the one hand, the downstream reflection coefficient R^- is equal to -1 , meaning that the pressure wave is fully reflected by the resonator group 2. On the other hand, the upstream no-reflection condition $R^+ = 0$ can be obtained by canceling the numerator of R^+ , leading to

$$\beta_1(f) = \frac{\tilde{Z}_1(f)}{N\tilde{Z}_0} = \frac{1}{1 + i \cot(k_0\delta)} \quad \Leftrightarrow \quad \frac{Z_1^c(f)}{Z_0} = \frac{NS_1}{S_w} \frac{1}{1 + i \cot(k_0\delta)}. \quad (12)$$

Discussion of the conditions for perfect absorption. The surface reactance of a resonator vanishes at its resonances. If there are no inner losses in a resonator, its surface resistance will vanish at any frequency and the perfect no-transmission condition Eq. (9) can be satisfied at the resonance frequencies of the resonator. However, in practice, the inner losses of a resonator are never zero. Its surface resistance cannot be exactly equal to zero while a zero surface reactance is still reached at the resonance frequencies of the resonator. The lowest transmission that can be achieved is limited by the surface resistance of the resonators and will depend on how well the Eq. (10) impedance condition is met. This way, for a given normalized surface impedance Z_2^c/Z_0 , the larger NS_2/S_w , the lower the transmission. This is the fundamental reason why reducing the transmission in narrow waveguides is easier than in wide waveguides. Note that duplicating the resonator group 2 and adjusting the new resonator group position can also greatly reduce the transmission, as described in Appendix A.3.1. Finally, while the resonator group 2 is responsible of canceling the transmission at a given frequency, the resonator group 1 also impacts the transmission at this frequency.

The resonators impedance of resonator group 1 leading to perfect no-reflection, Eq. (12), is proportional to the ratio NS_1/S_w and is governed by the distance δ and more precisely the dimensionless variable $k_0\delta$ as illustrated in Fig. 6. Moreover, Fabry–Perot interferences of the absorber are found whenever $k_0\delta = n\pi$ with $n \in \mathbb{N}$ (i.e., when $\delta = n\lambda/2$). These interferences imply $R^+ = -1$ for any value of Z_1^c : this particular spacing forbids high absorption [3]. Away from Fabry–Perot interferences, perfect no-reflection can be obtained as the target resistance is not null. The no-reflection condition can also be understood as an impedance matching between the characteristic impedance of the propagation line and the impedance at the x position of the resonator group 1 [12]: $(N\tilde{Z}_0)^{-1} = (iN\tilde{Z}_0 \tan(k_0\delta))^{-1} + (\tilde{Z}_1)^{-1}$.

Perfect absorption consists in reflection and transmission coefficients exactly equal to zero. In practice, the transmission coefficient is never exactly equal to zero but can be extremely close to zero. The reflection coefficient can be exactly equal to zero. Then, perfect absorption is the objective of the optimization problem.

The ratio between the area of the resonators surface connected to the propagation line NS_1 and NS_2 and the area of the propagation line cross-section S_w , is common to the quasi no-transmission and no-reflection conditions, Eqs. (10) and (12) and will appear in other expressions below. As it is an area ratio, it can be related to the leakage flux.

Merkel et al. [3], Jiménez et al. [5] and Long et al. [12] have designed asymmetric absorbers made of two HRs for perfect absorption at a single frequency by optimizing the absorbers parameters. The absorption is not predicted but explained *a posteriori* of the optimization. The pair of optimized HRs is found to be slightly detuned: the first resonance of resonator 2 f_2 such that $\Im(Z_2^c(f_2)) = 0$ occurs at slightly lower frequency than that of resonator 1, f_1 , where \Im denotes the imaginary part of a complex number. The origin of this slight detuning can be explained by Eqs. (9) and (12). Resonator 2 makes the transmission vanish at its resonance frequency, f_2 , Eq. (9). To cancel the reflection, the resonator 1 surface reactance must take a small value, Eq. (12). The surface reactance of resonator 1 is then low and, as the surface reactance of an HR or an homogeneously filled QWR monotonically increases until its first anti-resonance, $\Re(Z_1^c) = 0$ occurs at a frequency f_1 slightly different than f_2 . Resonators close to each other ($0 < k_0\delta < \pi/2$) implies that the optimal reactance for resonator 1 is negative at f_2 and thus $f_1 > f_2$. Conversely, $\pi/2 < k_0\delta < \pi$ leads to $f_2 > f_1$: the resonance of resonator 1 can occur at a lower frequency than that of resonator 2 while still respecting the perfect no-reflection condition. Long et al. [11] have also shown that the HRs forming an asymmetric absorber decorated for perfect absorption can be tuned at the same resonance frequency. This particular configuration occurs for $k_0\delta = \pi/2$.

Thus, two groups of point resonators (each group can be composed of a single resonator) separated by a distance δ can be designed for perfect absorption, with the surface impedance of the resonators of group 2 following Eq. (10) and that of group 1 following Eq. (12), as long as $k_0\delta \neq n\pi$. To avoid designing unnecessary long absorbers, $k_0\delta < \pi$ should be used.

4.1.2. Minimal absorber length

In many practical applications, the length of the absorber, l_A , must be as short as possible. Considering an absorber made of two different groups of resonators (see Fig. 4), if the surface impedance of the resonators can take any values at a given frequency, the length of the absorber $l_{AA} = \delta$, can be very small but has to remain greater than zero. In practice, the reachable values of impedance depend on the type of used resonator and on the resonator dimensions, as presented in Fig. 2 and discussed in Section 2.3.2 for QWRs filled with a micro-lattice. The no-transmission condition Eq. (9), or its approximation Eq. (10), does not depend on δ . For the group 2, it can be reached for instance by using a QWR filled with air and adjusting its height, or a HR filled with air and adjusting the dimensions of its neck and cavity. The no-reflection condition Eq. (12) depends on $k_0\delta$ and is usually harder to achieve because the surface resistance of the resonator must be of the order of NS_1/S_w , i.e., higher than zero but still very low. Its reactance is simpler to tune by varying the resonator height. Based on these considerations, at the targeted perfect absorption frequency, if the normalized surface resistance of the resonators composing the group 1 is written $\Re(Z_1^c/Z_0) = \Gamma$, where \Re denotes the real part of a complex number, and if the group 2 cancels the transmission, then achieving no-reflection requires

$$\Gamma = \frac{NS_1}{S_w} \sin^2(k_0\delta). \tag{13}$$

If $k_0\delta$ tends to zero, i.e., for low frequency and small δ , this expression can be approximated as

$$\delta = l_{A,min} = \frac{\lambda}{2\pi} \sqrt{\frac{\Gamma S_w}{NS_1}}, \quad \text{when } k_0\delta \ll 1. \tag{14}$$

This way, if the surface resistance of the group 1 resonators cannot be lower than a value Γ at the targeted perfect absorption frequency, the minimum distance between the resonators groups, which is by consequence the minimum absorber length, is approximated by Eq. (14). Thus, the minimum absorber length is governed by the targeted frequency or its corresponding wavelength in air λ , the ratio between the duct section and the resonators section $S_w/(NS_1)$, as well as the minimal reachable normalized resistance Γ at this frequency. Note that, as shown in Appendix A.3.2, increasing the number of resonator groups can help decrease the minimal absorber length but the main features highlighted in Eq. (14) are maintained.

In the literature, the length of duct liners, l_A , is often compared to the longest mostly absorbed wavelength in air, λ , or $\lambda/4$ [4]. It does not allow to make a fair difficulty of design comparison between the absorbers because, in the view of Eq. (14), it is clear that the λ/δ ratio strongly depends on the area of the waveguide cross section, S_w , and that the optimal impedance values are strongly linked to resonators and waveguide areas ratio, Eqs. (10) and (12). Moreover, multiple detuned resonators can be located at the same axial position [12] underlying the importance of accounting for the area covered by all the resonators instead of the length of the absorber.

Instead of comparing l_A to λ , we suggest comparing l_A to the length $\lambda\sqrt{S_w/S_A}$, with S_A being the total area of the walls of the waveguide covered by the absorber, i.e., the volume of the absorber divided by its height. This expression combines three dimensions: the acoustic wavelength, λ , the area of the cross section of the propagation line, S_w , and the area of the walls of the waveguide covered by the absorber, S_A . The height of the absorber is not included in this expression because there is no physical link between this height and the minimal length of the absorber.

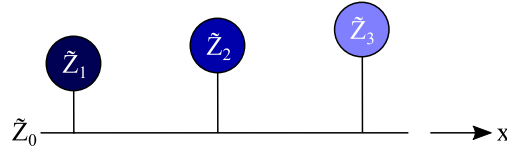


Fig. 7. Schematic representation of a 1D asymmetric absorber composed of three different groups of resonators ($N = 1$) able to perfectly absorb two arbitrary frequencies. Each resonator is located at a different axial position x .

4.2. Conditions for perfect absorption at multiple close frequencies

A pair of resonators can target unidirectional perfect absorption at a given frequency with one implementing the quasi-no-transmission impedance, Eq. (10) and with the other one satisfying the no-reflection impedance, Eq. (12). Targeting perfect absorption over a broad frequency range requires to couple absorption peaks resulting from a combination of more than two resonators.

Long et al. obtained four absorption peaks ($\alpha^+ \approx 94\%$) using eight different HRs placed in two groups of four HRs and two close absorption peaks with one reaching 100% using three different HRs placed at different axial positions [12]. Long et al. obtained $\alpha^+ > 95\%$ between 280 and 431 Hz by combining twelve HRs placed in four groups of three HRs [11]. Note that, as long as at least two different resonators are placed at different axial positions to break the propagation symmetry, placing different resonators at the same axial position is not fundamentally different from spacing the different resonators provided they are not interacting, see Appendix A.4. In addition, Guo et al. obtained four absorption peaks using five different HRs having an optimized separation distance [39].

The most straightforward way to target unidirectional perfect absorption at F frequencies, thus forming an asymmetric absorber for perfect multiband or broadband absorption, consists in putting together F pairs of resonators, with each pair being responsible for a single frequency. However, less than F pairs of resonators, i.e., $2F$ resonators, can be used while still reaching the same level of absorption at F frequencies. In fact, in an ideal case where resonators could take any surface impedance value at any frequency, perfect absorption for F frequencies could be achieved by a single pair of such resonators. In practice, the impedance of passive resonators such as HRs or QWRs is difficult or impossible to tune at several given frequencies simultaneously since the frequency dependence of the impedance is prescribed by the underlying physical mechanisms. In particular, standard resonators such as HRs and QWRs filled with air can only fulfill the quasi-no-transmission Eq. (10) at their resonance frequencies. The transmission is also reduced around the resonance frequencies and the thinner the waveguide, the stronger and the broader the attenuation. If the frequencies targeted by the broadband asymmetric absorber are arbitrary and the width of the duct is of the order of centimeters, then there should be at least F resonators to cancel the transmission at F frequencies. A multi-order resonator, i.e., a resonator composed of multiple resonant elements [13], should be considered as O resonators with O being the resonator order. The no-reflection impedance condition Eq. (12), with δ being the distance between the two resonators responsible for a given frequency, is slightly modified if other resonators are located between these two resonators. However, the necessity remains to reach a certain non-zero surface impedance that depends on $k_0\delta$ to cancel the reflection. It can be reached at multiple frequencies by a single resonator. Then, the number of resonators of the broadband asymmetric absorber lining a duct having a width of the order of centimeters should at least be equal to $F + 1$ and can be lower than $2F$. The absorber shown in Fig. 7 made of three resonators can thus target perfect absorption at two distinct frequencies.

Tuning the distances between the resonators and using a type of resonators whose surface impedance can be easily adjusted at several frequencies help in reducing the required number of resonators.

A minimum of $F + 1$ resonators is needed to reach unidirectional perfect absorption. To simultaneously reach perfect absorption from both sides of the system at the same frequency the absorber can be symmetrized around the last resonator. The absorber is then mirror symmetric and composed of $2F + 1$ resonators [3]. This number can be reduced in the best realistic scenario to $F + 2$ resonators because F resonators are required to cancel the transmission at F frequencies and 1 resonator is required to cancel the reflection in each direction for all frequencies. The resonator canceling R^+ is placed at the beginning of the absorber and the resonator canceling R^- is placed at the end of the absorber.

It is also important to note that every resonator impacts the reflection and transmission coefficients of the absorber at all frequencies. The increase of the number of resonators composing an absorber facilitates the obtaining of a high absorption and complicates the obtaining of the perfect no-reflexion.

5. Optimization in realistic conditions

Based on the TMM analysis presented in the previous section, it is possible to target perfect absorption at a single and at multiple frequencies by means of porous asymmetric absorbers. Moreover, the length of the absorbers could potentially be shorter than $\lambda/4$, provided the waveguide cross-section is not too large and its height is lower than $\lambda/4$ using folded QWRs. In this section, the porous absorbers are optimized using the more detailed MMT in order to show that the key results obtained with the TMM are still valid when possible coupling between the QWRs are accounted for.

Table 1

Optimized parameters and corresponding normalized surface impedances of absorbers made of two QWRs of length $l_{1,2} = 5$ mm, separated by a rigid wall of length δ_r and lining a (x, y) wall of a waveguide of height h_w . The width of the QWRs is equal to that of the waveguide, $w_1 = w_2 = w_w = 5$ mm.

h_w (mm)	δ_r (mm)	IF_1 (%)	h_1 (mm)	Z_1/Z_0 (2700 Hz)	IF_2 (%)	h_2 (mm)	Z_2/Z_0 (2700 Hz)
10	100	33.4	27.8	$0.40 + 0.18i$	Air	30.0	$0.02 - 0.06i$
20	5	8.5	26.4	$0.05 - 0.20i$	Air	29.7	$0.02 - 0.08i$
40	5	Air	28.4	$0.02 - 0.15i$	Air	29.9	$0.02 - 0.08i$

5.1. Single frequency optimization

Absorbers made of two straight ($\xi = 0$) QWRs are optimized for three different configurations. The absorbers cover a single (x, y) wall of the waveguides. The lengths l_1 and l_2 of the QWRs are set to 5 mm. For simplicity, the cross section of the QWRs is square: the width of the QWRs is equal to their length, $w_1 = w_2 = 5$ mm. To keep the visco-thermal losses negligible in the main duct at the frequency range of interest, its width is $w_w = 10$ mm. In order to fully cover the (x, y) wall of the waveguide forming the absorber, the QWRs are duplicated in the transverse direction of the waveguide y . Their height h_1 and h_2 and the IF of their filling micro-lattice are optimized to maximize the absorption at $f = 2700$ Hz corresponding to a wavelength in air $\lambda = 127$ mm. For the MMT predictions, 25 and 2 modes were used in the z and y directions, respectively. Maximizing the absorption coefficient α^+ is performed with the iterative Nelder–Mead algorithm [40] which is a heuristic direct search method implemented in the Matlab function *fminsearch*.

The first configuration aims to illustrate the validity of the TMM analysis to predict optimal impedances. It consists in a $h_w = 10$ mm waveguide and a long axial rigid section separating the QWRs of $\delta_r = 100$ mm. The optimized parameters and the resulting QWRs surface impedances, Z_1 and Z_2 , are summarized in Table 1 and $\alpha^+(f = 2700 \text{ Hz}) = 100\%$. As expected, the second QWR is filled with air and has a sufficiently low surface impedance to strongly diminish the transmission, see Eq. (10). The TMM analysis led to the expression (12) for the impedance of the first resonator while the second resonator makes the transmission vanish. As summarized in Table 2, in the considered case, the TMM predicted an optimal impedance $Z_1^c/Z_0 = 0.39 + 0.20i$. For the MMT optimized absorber, the normalized surface impedance of the first QWR is close to this value with $Z_1/Z_0 = 0.40 + 0.18i$. Note that this last impedance value is not adjusted by a length correction because no length correction is needed in the MMT. In addition to the impact of the length correction, the small impedance difference with the TMM prediction may come from the fact that the second QWR does not perfectly makes the transmission vanish. Another explanation is that a coupling still occurs between the two resonators, despite the large distance δ_r between them, or that the resonators are too large to be perfectly modeled as point resonators.

The second and third configurations are more realistic: the distance between the two QWRs is reduced to $\delta_r = 5$ mm so that the total length of these absorbers is $15 \text{ mm} = \lambda/8.5$. The waveguide height is increased to either $h_w = 20$ mm or $h_w = 40$ mm. Their optimized parameters and the resulting QWRs surface impedances are summarized in Table 1 and their corresponding absorption coefficients are shown in Fig. 8 by the blue solid line and black dot-dashed line, respectively. For the $h_w = 20$ mm waveguide the absorber is able to reach $\alpha^+(f = 2700 \text{ Hz}) = 100\%$. In contrast, for the larger waveguide ($h_w = 40$ mm) the absorber achieves $\alpha^+(f = 2700 \text{ Hz}) = 90\%$ with a narrower absorption peak. In these configurations, the optimal impedance of the first resonator predicted by the TMM, Eq. (12), and summarized in Table 2 is less accurate than in the first configuration. This is because the resonators are close to each other and thus most probably coupled. However, this equation still highlights that a large ratio S_w/S_1 requires low Z_1 that might not be reached by the available porous material. It is the case for the $h_w = 40$ mm waveguide which results in an optimized first QWR filled with air. The surface impedance of the first QWR is then solely governed by the height of the QWR and its fixed (and thus not tuned) cross-section. Conversely, the first QWR optimal impedance for the $h_w = 20$ mm waveguide can be attained by filling it with a tuned micro-lattice and $\alpha^+ = 100\%$ is then reached.

These optimizations based on a propagation model that includes the potential coupling between the resonators confirm that, just as HRs, straight QWRs filled with homogeneous media (air or porous materials) can be used to target perfect absorption in a ducted propagation problem. The QWR placed the farthest from the incident wave is filled with air to obtain very low intrinsic losses. The transmission vanishes at the resonance frequency of the resonator. The QWR closer to the incident wave is filled with a porous medium with a controlled pore size. This way, its intrinsic losses are adjusted such that the absorber made of the two QWRs is impedance-matched with the waveguide [12], leading to no reflection. As underlined by Eq. (14), the length of the resulting absorber can be smaller than a quarter-wavelength in air at the fully absorbed frequency. These optimizations also show that the simple expressions (9) and (12) for the optimal impedances, derived considering no coupling between the resonators, give good trends of the actual optimal impedances and reliable predictions for large spacing between the resonators. Finally, these optimizations highlight that the critical parameter controlling the minimal absorber length is not only the wavelength but also the ratio between the waveguide section and the resonators section.

5.2. Optimization for two close frequencies

To target perfect unidirectional absorption at two close frequencies $f = 2700$ Hz and 3000 Hz, an absorber composed of three straight ($\xi = 0$) QWRs is optimized. A $h_w = 20$ mm and $w_w = 10$ mm waveguide is considered and $w_1 = w_2 = w_3 = l_1 = l_2 = l_3 = 5$ mm.

Table 2

Optimal corrected surface impedances for perfect absorption at 2700 Hz, according to the TMM analysis assuming point resonators. The absorbers are made of two QWRs of length $l_{1,2} = 5$ mm, separated by a rigid wall of length δ_r and lining a (x, y) wall of a waveguide of height h_w . The width of the QWRs is equal to that of the waveguide, $w_1 = w_2 = w_w = 5$ mm.

h_w (mm)	δ_r (mm)	δ (mm)	Z_1^c/Z_0 , Eq. (12) (2700 Hz)	Z_2^c/Z_0 , Eq. (9) (2700 Hz)
10	100	105	0.39 + 0.20i	0.00 + 0.00i
20	5	10	0.06 - 0.10i	0.00 + 0.00i
40	5	10	0.03 - 0.05i	0.00 + 0.00i

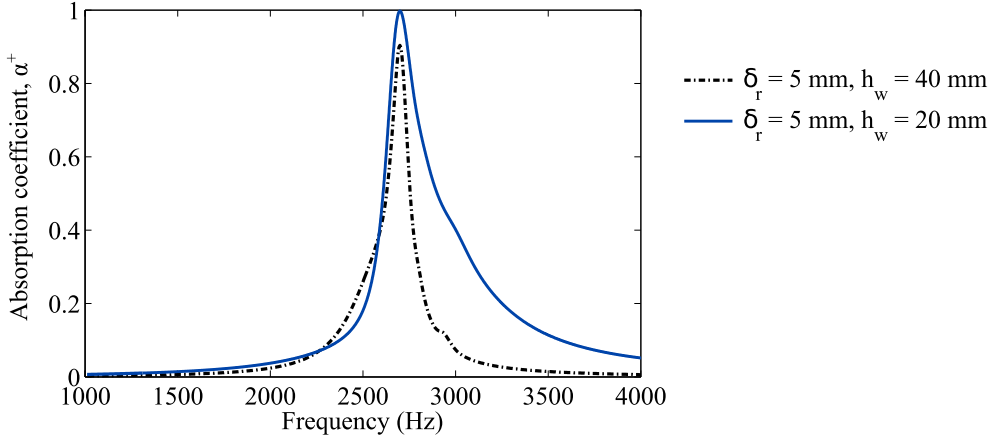


Fig. 8. (color online) MMT predicted absorption coefficient of the optimized absorbers made of two QWRs of length $l_{1,2} = 5$ mm and separated by a rigid wall of length $\delta_r = 5$ mm. The waveguide height is $h_w = 20$ mm (blue solid line) or 40 mm (black dot dashed line).

Table 3

Optimized parameters of the absorbers for maximizing α^+ at 2700 Hz and 3000 Hz, made of three QWRs of length $l_{1,2,3} = 5$ mm, separated by δ_r , rigid walls and lining a (x, y) wall of a $h_w = 20$ mm high waveguide. The width of the QWRs is equal to that of the waveguide, $w_1 = w_2 = w_3 = w_w = 5$ mm and $\bar{\alpha} = (\alpha(2700 \text{ Hz}) + \alpha(3000 \text{ Hz}))/2$.

δ_r (mm)	IF_1 (%)	h_1 (mm)	IF_2 (%)	h_2 (mm)	IF_3 (%)	h_3 (mm)	$\bar{\alpha}$
5.0	20	23.7	Air	30	Air	28.2	0.870
29.0	27.8	23.7	Air	25.6	Air	28.6	0.996
20.0	28.2	23.7	Air	28.6	Air	25.6	0.995

As in the configuration described in Section 5.1, the QWRs are duplicated in the transverse direction of the waveguide. First, the parameters $h_1, h_2, h_3, IF_1, IF_2, IF_3$ of the absorber are optimized for a rigid separation distance $\delta_r = 5$ mm between each QWR. The optimized parameters are given in Table 3 and the corresponding absorption coefficient is shown in Fig. 9 by a black dot-dashed line. The second and third QWRs are filled with air and cancel the transmission at the two targeted frequencies. The first QWR is filled with a micro-lattice and is not able to cancel perfectly the reflection at both frequencies. It means that with $\delta_r = 5$ mm, the optimal impedance for the first QWR cannot be realized at these two frequencies with the considered filling porous medium. This behavior was already observed in [12] where three HRs with fixed axial separation distance could not reach very high absorption at two frequencies.

In a second stage, the distance δ_r is also optimized, either forcing $h_2 < h_3$ or forcing $h_2 > h_3$. The optimized parameters are given in Table 3 and the corresponding absorption coefficients are depicted in Fig. 9 by the blue solid line and red dashed line, respectively. In both cases, considering δ_r as an additional optimization parameter allows to reach $\alpha^+ > 99.5\%$ at the two targeted frequencies. The surface impedance of the first porous QWR is matched to the optimal one. The axial position of the tallest QWR filled with air (i.e., the QWR making the transmission vanish at the lowest frequency) does not determine if $\alpha^+ = 100\%$ can be reached or not but it does influence the optimal δ_r and slightly influence the optimal IF_1 . The advantage of optimizing δ_r was already noted in [39,41] where 5 HRs with optimized axial separation distance could reach very high absorption at 4 frequencies. However, in the mentioned work, the total length of the optimized absorber is larger than 1 m. Since the optimal surface impedance for the resonator responsible for canceling the transmission, Eq. (12), is $k_0\delta/\pi$ periodic, δ can be reduced as long as $\delta \bmod \pi/k_0$ is not modified and as long as the coupling between the resonators is moderate.

Asymmetric sound absorbers made of QWRs for perfect absorption at multiple frequencies can thus be designed. The analysis of the system by means of TMM highlights that the minimal number of resonators to fully absorb F arbitrary frequencies is $F + 1$, as was illustrated by the $\alpha^+ > 99.5\%$ at two frequencies obtained by three QWRs. No clear rule could be derived for the positioning of

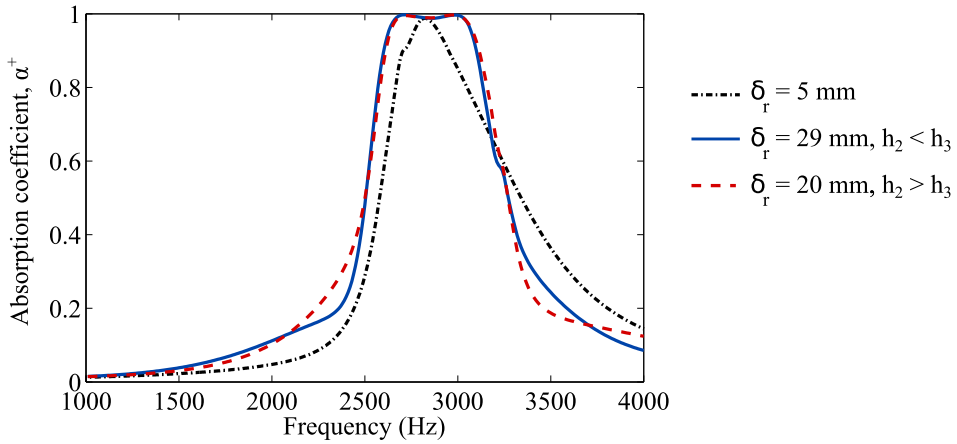


Fig. 9. (color online) MMT predicted absorption coefficient of the optimized absorbers three QWRs of length $l_{1,2,3} = 5$ mm. The waveguide height is 20 mm and the QWRs are separated by rigid walls of length $\delta_r = 5$ mm (black dot dashed line), 20 mm (red dashed line) or 29 mm (blue solid line).

the resonators responsible for canceling the transmission in function of the frequency. A more advanced type of porous absorber is presented in the following section.

5.3. Broad target frequency bandwidth and sub-wavelength absorption

Finally, an Asymmetric Broad target frequency bandwidth Sub-wavelength Absorber (ABSA) made of folded ($\xi \geq 0$) QWRs filled with micro-lattices or air is optimized for perfect absorption. The proposed ABSA has a length $l_{ABSA} = 200$ mm, a width of 50 mm and is composed of folded QWRs of height $h_{ABSA} = 30$ mm. It lines the bottom wall of a waveguide of height $h_w = 40$ mm and width $w_w = 50$ mm, see Fig. 10(a). Its open area ratio is then $h_w / (h_w + h_{ABSA}) = 0.57$. It is composed of 12 distinct and closely packed folded QWRs in the axial direction of the waveguide. These QWRs are duplicated 3 times along the width of the waveguide. After various numerical tests, it was found that a combination of 3 QWRs to make the reflection vanish and 9 QWRs to make the transmission vanish gave the most satisfactory results. The QWRs 1 to 3 are responsible for canceling the upstream reflection, R^+ . They are filled with bi-layer micro-lattices to provide more freedom to tune their surface impedance and thus realize the optimal surface impedance at multiple frequencies. The QWRs 4 to 12 are filled with a homogeneous micro-lattice or with air and are responsible for canceling the transmission. Obviously, QWRs 1 to 3 also have an impact on the transmission and QWRs 4 to 12 also have an impact on the reflection.

5.3.1. Optimization

The ABSA is optimized to maximize its absorption coefficient over the frequency range $f \in [1250; 2150]$ Hz, evenly discretized by 24 points. The optimization is performed in two steps due to the large number of optimization parameters. The folded QWRs labeled 4 to 12 responsible for canceling the transmission are first considered and optimized by minimizing the cost function

$$J_T = \sum_f |T(f)|^2. \quad (15)$$

Then, in a second step, all the QWRs (1 to 12) are considered and optimized. The QWRs 4 to 12 are initialized with the values found during the first optimization step. The cost function J_{RT} for this second stage is

$$J_{RT} = \sum_f |R^+(f)|^2 + |T(f)|^2. \quad (16)$$

The optimized parameters for QWRs 4 to 12 are their ξ and IF. For QWRs 1 to 3, the optimized parameters are their ξ , the IF of the two layers named IF_1 and IF_2 and the height of layer 1, h_1 , layer 1 being the bottom layer. As the height of the folded QWRs is fixed and equal to h_{ABSA} , the height of layer 2 is $h_2 = h_{ABSA} - h_1$. The MMT is still used for the predictions of the acoustic behavior of the absorber during the optimization.

The main role of the resonators can be verified numerically after their optimization. For instance, only considering the optimized QWRs 4 to 12 leads to a low transmission and a non controlled reflection in the frequency range of interest.

The optimized parameters of the ABSA are summarized in Table 4 and the corresponding acoustic behavior is presented in Fig. 11 in terms of (a) the absorption coefficient α^+ , (b) the transmission loss $TL = -20 \log(|T|)$ and (c) $RL = -20 \log(|R^+|)$. The reflection and transmission coefficients are expressed in dB to highlight the differences at low absolute values. There is good agreement between the MMT predictions (dot-dashed black lines) and the FEM validation (solid blue lines). The small discrepancies in frequency and level can be ascribed to the simplified geometry of the folded porous QWRs when predicting their surface impedance used by the MMT. The FEM model predicts an absorption coefficient $\alpha^+ \in [98.8; 99.6]\%$ over the frequency range $f \in [1255; 2130]$ Hz with a

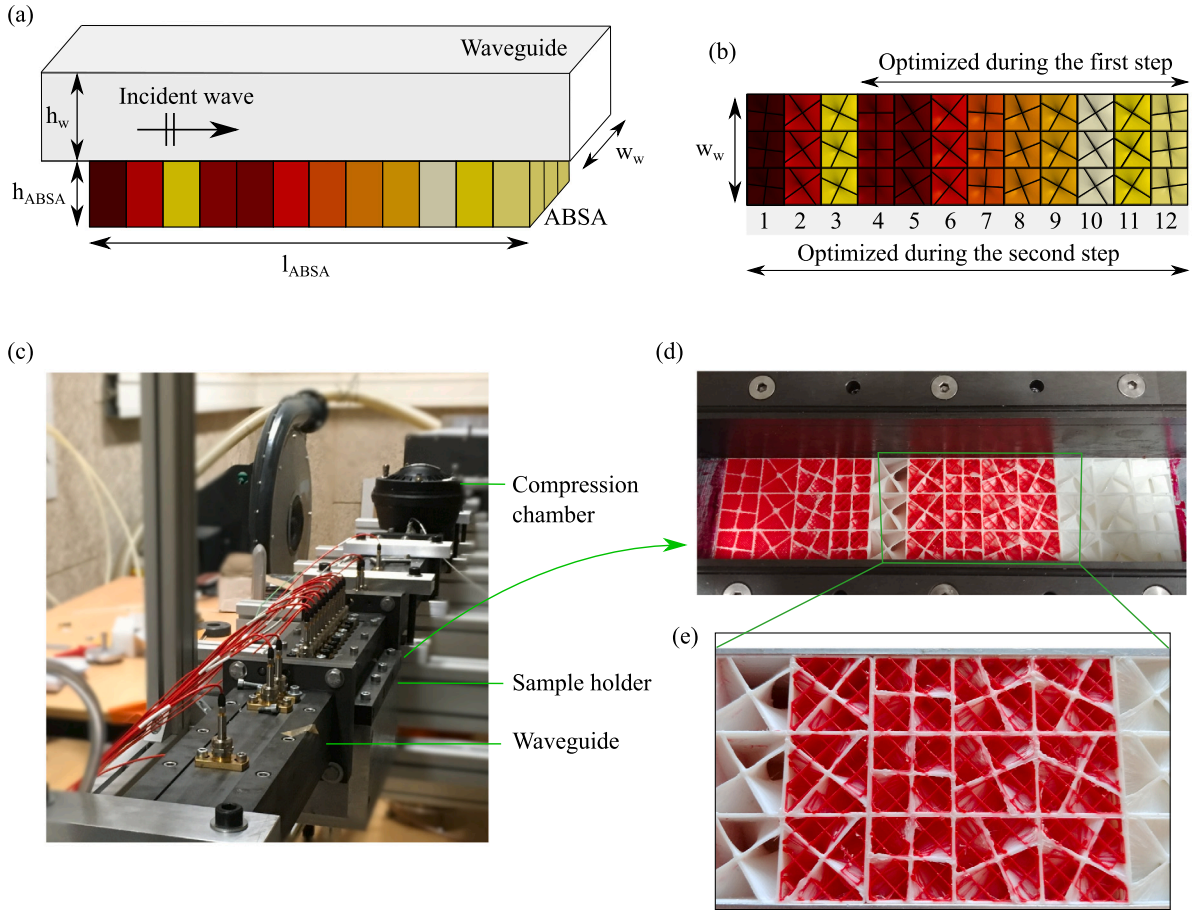


Fig. 10. (color online) ABSA of length $l_{ABSA} = 200$ mm and height $h_{ABSA} = 30$ mm, flush mounted on a waveguide of height $h_w = 40$ mm and optimized for maximal average absorption over $f \in [1250; 2150]$ Hz. (a) Numerical perspective view of the ABSA lining the waveguide. (b) Numerical top view of the ABSA. (c) Picture of the duct test bench. (d) Picture of the 3D printed sample mounted in the duct test bench. (e) Picture of the 3D printed sample, close-up view.

mean value of $\bar{\alpha}^+ = 99.2\%$. The TL and the RL are comprised between 20 dB and 40 dB. The frequency $f = 1255$ Hz corresponds to a wavelength in air of $\lambda = 273$ mm. The absorber is therefore sub-wavelength with respect to its height with $h_{ABSA} = \lambda/9.1$. Its length is such that $l_{ABSA} = \lambda/1.4$. Following the discussion in Section 4.1.2, $l_{ABSA} = \lambda \sqrt{S_w/S_{ABSA}}/0.61$.

For frequencies lower than $f = 1255$ Hz both TL and α^+ drop towards 0. No resonator has a surface impedance close enough to zero required to cancel the transmission, Eq. (9). Conversely, the RL exhibits sharp peaks at null frequency and $f = 666$ Hz due to the 0th and 1st Fabry–Pérot interferences associated to the length 200 mm of the ABSA [3]. For frequencies above 2130 Hz, the TL and RL are low and start to oscillate for frequencies greater than 3×1255 Hz (α^+ follows a similar trend). These oscillations are due to the resonator dynamics bringing their surface impedances close to optimal values for no transmission and no reflection because the impedances of QWRs take similar values around the QWRs first, third, fifth... quarter-wavelength frequencies, see Fig. 2.

The designed and optimized ABSA is the first compact absorber to achieve $\alpha^+ > 99\%$ over a broad target frequency bandwidth while lining a waveguide of the order of centimeters wide. The absorber is compact in the sense that the resonators forming the ABSA are closely packed.

5.3.2. Experimental validation

We now describe the manufacturing process of the optimized ABSA and its acoustic testing in a rectangular duct with grazing incident waves.

The folded QWRs composing the ABSA are 3D printed using Fused Deposition Modeling (FDM) technique. In addition to the 200 μm diameter nozzle responsible for the manufacturing of the micro-lattices (see Section 2.2), a 400 μm diameter nozzle is responsible for the manufacturing of the rigid structures (vertical and helical walls). Four blocks of 3×3 folded QWRs are manufactured separately and assembled with vacuum grease on their external walls in the duct sample holder as depicted in Fig. 10(c) and (d).

Table 4
Parameters of the folded QWRs composing the optimized ABSA of height $h_{ABSA} = 30$ mm.

Resonator	ξ	Layer 1 height (mm)	Layer 2 height (mm)	Simulation		Manufacture	
				IF_1 (%)	IF_2 (%)	IF_1 (%)	IF_2 (%)
1	0.27	24	6	30	29	26	25
2	0.65	9	21	28	25	34	21
3	1.57	9	21	15	9	12	6
4	0.50	30	–	10	–	7	–
5	0.41	30	–	Air	–	Air	–
6	0.86	30	–	8	–	5	–
7	1.01	30	–	8	–	5	–
8	1.19	30	–	7	–	4	–
9	1.33	30	–	9	–	6	–
10	1.91	30	–	Air	–	Air	–
11	1.59	30	–	Air	–	Air	–
12	1.73	30	–	Air	–	Air	–

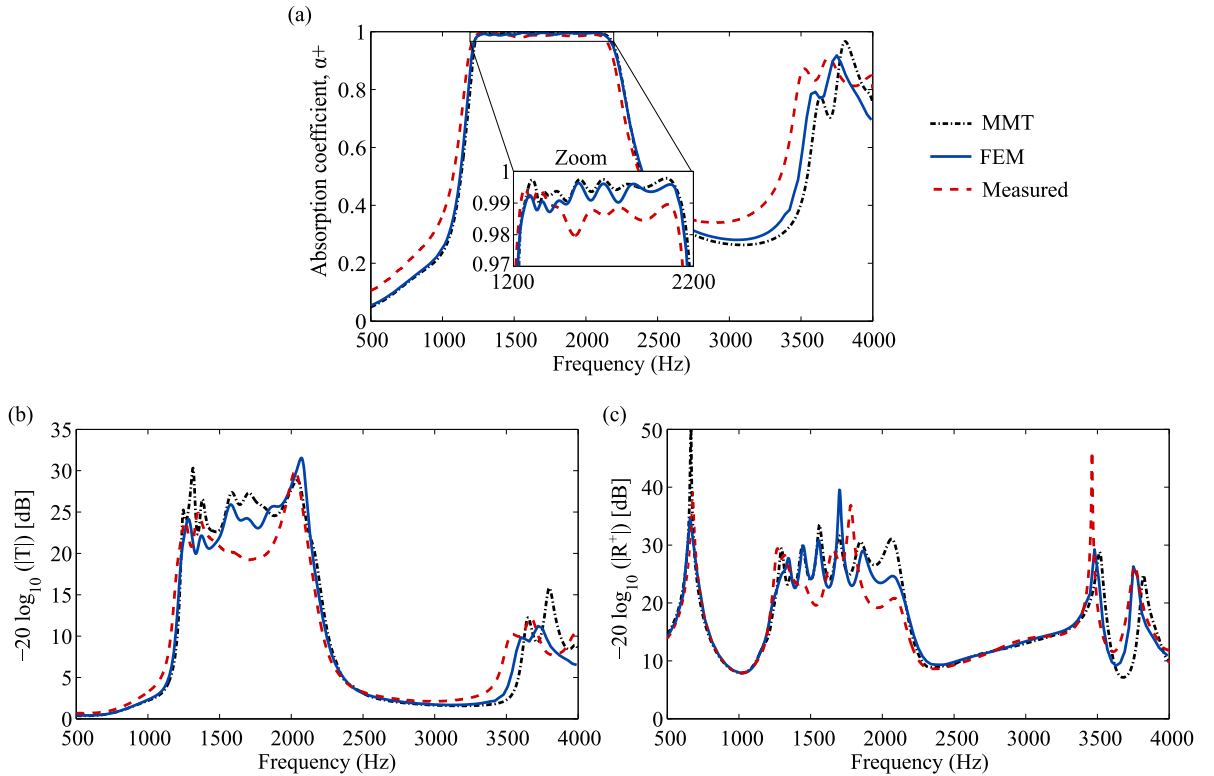


Fig. 11. (color online) Acoustic behavior of the optimized ABSA. Simulations with the MMT (black dot-dashed lines) and with FEM (blue solid lines), measurements (red dashed lines). (a) Absorption coefficient α^+ . (b) Transmission loss $-20 \log_{10}(|T|)$. (c) $-20 \log_{10}(|R^+|)$.

When the folded QWRs are filled with micro-lattices, the losses of the walls of the QWRs are neglected in all models. Experimentally, these additional losses can be approximately compensated by slightly decreasing the losses of the filling micro-lattices. To do so, their lattice constant is increased. More precisely, IF is decreased so that the micro-lattice porosity is increased by 0.03. This small value originates from the validation tests reported in [33]. The manufacturing parameters of the optimized ABSA are summarized in Table 4.

The manufactured ABSA is mounted in the wall of a rectangular duct of inner height $h_w = 40$ mm and width $w_w = 50$ mm ended by an anechoic termination. This experimental facility and the associated measurement techniques have already been introduced and detailed in [42]. On each side of the sample, three microphones are placed and permit the measurements of the R^+ and T coefficients using a scattering matrix formalism. To that end, acoustic plane waves are generated by a compression chamber that can be mounted either upstream or downstream of the measurement section. The acoustic signal consists of a sine sweep going from 500 to 4000 Hz with a step of 2 Hz. The incident pressure wave amplitude is set to 90 dB at each frequency.

The measured acoustic behavior of the ABSA is represented in Fig. 11 by red dashed lines. There is a good correlation between the measured and the predicted results. The experimental performance is slightly lower than predicted in the targeted frequency

range, and slightly higher for lower and higher frequencies. The small differences between the measured coefficients and those predicted by FEM may come mainly from the imperfection of the 3D printing, leading in particular to walls thicker than expected. The mounting of the sample in the duct can also induce some supplementary and undesired reflections. Nevertheless, the measured data are still very close to the predicted results, demonstrating the relevance of the proposed design. In particular, the manufactured ABSA sample is able to deliver an absorption coefficient $\alpha^+ \in [98.0; 99.5]\%$ in the frequency range [1225; 2120] Hz, corresponding to a mean of value $\bar{\alpha}^+ = 98.7\%$, while the TL and RL values vary between 19 and 37 dB.

This work considers no air flow in the main duct. Measurements of the ABSA with air flow are reported in [43].

6. Conclusions

This work explores perfect, broad target frequency bandwidth and sub-wavelength acoustic absorption in waveguides of centimetric wide and constant cross section with porous asymmetric absorbers. A theoretical analysis based on the TMM provides insight and practical conditions for the understanding and design of such absorbers under the first cut-off frequency of the waveguide. Numerical simulations and experimental proof-of-concept illustrate that the theoretical results can be put into practice.

An asymmetric absorber is made of at least two resonators, the resonator farther from the incident wave cancels the transmission while the closer one implements an impedance match leading to no reflection. The no-transmission and no-reflection conditions are expressed in terms of the resonators surface impedances. The no-transmission condition is fulfilled by a zero impedance which can only be quasi-perfectly reached in practice due to the resonators losses. The no-reflection condition can be perfectly fulfilled by a non-zero impedance that depends on the spacing between the resonators and the target frequency. In both cases, the larger the ratio between the areas of the waveguide cross section and the resonator sections, the more difficult it is to reach the optimal impedances. In addition, scaling the system is not straightforward as the impedance of the resonators forming the absorber depend on their geometrical dimensions and the optimal no-reflection impedance depend on the spacing of the resonators.

The length of an asymmetric absorber, i.e., the distance in the propagation direction, optimized for perfect absorption, can be strongly smaller than a quarter of the wavelength in air when using straight quarter-wavelength resonators filled with homogeneous media. Conversely, the height of an absorber made of such resonators cannot be sub-wavelength because no transmission is attained at resonant frequencies of the resonators. The height of an asymmetric porous absorber can be rendered sub-wavelength, for instance using folded quarter-wavelength resonators.

Broadband and very high absorption can be obtained by combining pairs of resonators responsible for absorbing different close frequencies, thus forming a rippled plateau of absorption. The minimal number of resonators to cancel F arbitrary frequencies is $F + 1$, with F resonators canceling the transmission, located at the same or at different axial positions, and one resonator canceling the reflection placed at a different location than the resonators canceling the transmission.

Finally, a compact porous Asymmetric Broad target frequency bandwidth Sub-wavelength Absorber (ABSA) made of folded quarter-wavelength resonators is designed, optimized numerically, 3D printed and tested experimentally. A mean absorption coefficient of 99% is obtained experimentally over almost an octave and for frequencies smaller than the quarter-wavelength corresponding to the height of the absorber.

CRedit authorship contribution statement

Jean Boulvert: Conceptualization, Methodology, Software, Validation, Formal analysis, Investigation, Writing – original draft, Writing – review & editing, Visualization. **Thomas Humbert:** Investigation, Data curation, Writing – original draft, Writing – review & editing. **Vicente Romero-García:** Conceptualization, Methodology, Formal analysis, Writing – original draft, Writing – review & editing, Supervision. **Gwénaél Gabard:** Conceptualization, Methodology, Formal analysis, Writing – review & editing, Supervision, Project administration, Funding acquisition. **Edith Roland Fotsing:** Conceptualization, Writing – review & editing, Supervision. **Annie Ross:** Conceptualization, Formal analysis, Writing – review & editing, Supervision, Project administration, Funding acquisition. **Jacky Mardjono:** Conceptualization, Formal analysis, Writing – review & editing, Supervision, Project administration, Funding acquisition. **Jean-Philippe Groby:** Conceptualization, Methodology, Formal analysis, Writing – review & editing, Supervision.

Declaration of competing interest

The authors declare that they have no known competing financial interests or personal relationships that could have appeared to influence the work reported in this paper.

Acknowledgments

The authors acknowledge the financial support from the ANR industrial chair MACIA (ANR-16-CHIN-0002). They also acknowledge Safran Aircraft Engines and the Natural Sciences and Engineering Research Council of Canada (NSERC) for supporting and funding this research.

Appendix A. Transfer matrix method

A.1. Presentation of the method

A transfer matrix \mathbf{M} links the pressure p and axial flux v_x at two different positions along a transmission line [5]. For instance, between x and $x + \delta$ we write

$$\begin{bmatrix} p \\ v_x \end{bmatrix}_x = \mathbf{M} \begin{bmatrix} p \\ v_x \end{bmatrix}_{x+\delta}. \quad (\text{A.1})$$

The transfer matrix of a rigid section of the propagation line of length δ and of cross-sectional area S_w is

$$\mathbf{M}_\delta = \begin{bmatrix} c & i\tilde{Z}_0 s \\ is/\tilde{Z}_0 & c \end{bmatrix}, \quad (\text{A.2})$$

with $s = \sin(k_0\delta)$, $c = \cos(k_0\delta)$ and $\tilde{Z}_0 = Z_0/S_w$. The following is the transfer matrix for the i th point resonator with a surface impedance Z_i^c (corrected by a length correction) and with a cross-sectional area connected to the propagation line S_i :

$$\mathbf{M}_i = \begin{bmatrix} 1 & 0 \\ 1/\tilde{Z}_i & 1 \end{bmatrix}, \quad (\text{A.3})$$

where $\tilde{Z}_i = Z_i^c/S_i$. The transfer matrix for the i th resonator group composed of N_i identical point resonators with a surface impedance Z_i^c and with a cross-sectional area connected to the propagation line S_i is

$$\mathbf{M}_{g,i} = \begin{bmatrix} 1 & 0 \\ N_i/\tilde{Z}_i & 1 \end{bmatrix}, \quad (\text{A.4})$$

The transfer matrix of an absorber made of K resonator groups evenly spaced by a distance δ is

$$\mathbf{M}_a = \prod_{i=1}^K \mathbf{M}_{g,i} \mathbf{M}_\delta. \quad (\text{A.5})$$

The R^+ , R^- and T coefficients of the absorber are then given by

$$R^+ = \frac{\mathbf{M}_a(1,1) - \mathbf{M}_a(2,2) + \mathbf{M}_a(1,2)/\tilde{Z}_0 - \mathbf{M}_a(2,1)\tilde{Z}_0}{\mathbf{M}_a(1,1) + \mathbf{M}_a(2,2) + \mathbf{M}_a(1,2)/\tilde{Z}_0 + \mathbf{M}_a(2,1)\tilde{Z}_0}, \quad (\text{A.6})$$

$$R^- = \frac{-\mathbf{M}_a(1,1) + \mathbf{M}_a(2,2) + \mathbf{M}_a(1,2)/\tilde{Z}_0 - \mathbf{M}_a(2,1)\tilde{Z}_0}{\mathbf{M}_a(1,1) + \mathbf{M}_a(2,2) + \mathbf{M}_a(1,2)/\tilde{Z}_0 + \mathbf{M}_a(2,1)\tilde{Z}_0}, \quad (\text{A.7})$$

$$T = \frac{2e^{ik_0K\delta}}{\mathbf{M}_a(1,1) + \mathbf{M}_a(2,2) + \mathbf{M}_a(1,2)/\tilde{Z}_0 + \mathbf{M}_a(2,1)\tilde{Z}_0}. \quad (\text{A.8})$$

A.2. Absorber made of two resonator groups

We consider the case of an absorber composed of two distinct resonator groups separated by a distance δ . Each group is composed of N resonators. The transfer matrix corresponding to these two groups of resonators is

$$\mathbf{M}_a = \mathbf{M}_1 \mathbf{M}_\delta \mathbf{M}_2 = \begin{bmatrix} c + is \frac{N\tilde{Z}_0}{\tilde{Z}_2} & i\tilde{Z}_0 s \\ \frac{cN}{\tilde{Z}_2} + \frac{cN}{\tilde{Z}_1} + \frac{isN^2\tilde{Z}_0}{\tilde{Z}_1\tilde{Z}_2} + \frac{is}{\tilde{Z}_0} & c + is \frac{N\tilde{Z}_0}{\tilde{Z}_1} \end{bmatrix}. \quad (\text{A.9})$$

A.3. Absorber made of several resonator groups, with some of them being identical

A.3.1. Two identical resonator groups to make the transmission vanish

We consider the case where the two groups of resonators of an absorber are identical and composed of N identical resonators. The groups are separated by a distance δ and are used to make the transmission vanish. The transfer matrix corresponding to these two resonator groups is

$$\mathbf{M}_a = \mathbf{M}_2 \mathbf{M}_\delta \mathbf{M}_2 = \begin{bmatrix} c + is \frac{N\tilde{Z}_0}{\tilde{Z}_2} & i\tilde{Z}_0 s \\ \frac{2cN}{\tilde{Z}_2} + \frac{isN^2\tilde{Z}_0}{\tilde{Z}_2^2} + \frac{is}{\tilde{Z}_0} & c + is \frac{N\tilde{Z}_0}{\tilde{Z}_2} \end{bmatrix}. \quad (\text{A.10})$$

The corresponding transmission coefficient is

$$T = 2e^{ik_0\delta} [c(2 + 2\beta_2^{-1}) + is(2 + 2\beta_2^{-1} + \beta_2^{-2})]^{-1}. \quad (\text{A.11})$$

Therefore, if $\beta_2 < 1$ the transmission can be much lower than when using a single resonator group to cancel the transmission, Eq. (10). This is due to the term with the square of β_2 in the expression for T for two identical resonator groups, Eq. (A.11).

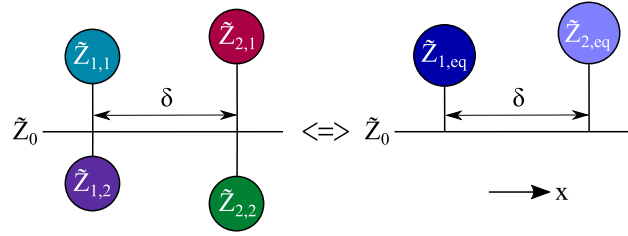


Fig. A.12. Schematic representation of a 1D asymmetric absorber composed of two pairs of different resonators. Each pair is composed of two different resonators located at a given x position. The pairs are separated by a distance δ .

A.3.2. One resonator group to cancel the transmission and two identical resonator groups to cancel the reflection

We consider an absorber that is composed of three resonator groups. Each group is formed of N identical resonators. The first and second resonator groups are identical and different that the third resonator group. The transfer matrix of this absorber is

$$\mathbf{M}_a = \mathbf{M}_1 \mathbf{M}_\delta \mathbf{M}_1 \mathbf{M}_\delta \mathbf{M}_3. \quad (\text{A.12})$$

If the third resonator groups is designed to make the transmission vanish, $Z_3/Z_0 = 0$, a new target impedance for the resonator group responsible for making the reflection R^+ vanish can be written as

$$\frac{Z_1^{c,\pm}}{Z_0} = \frac{NS_1}{S_w} \frac{2}{1 + 3i \cot(k_0\delta) \pm \sqrt{\Delta}}, \quad \text{with } \sin(k_0\delta) \neq 0 \text{ and } \Delta = (1 + 3i \cot(k_0\delta))^2 + 4 \frac{e^{-2ik_0\delta}}{\sin^2(k_0\delta)}. \quad (\text{A.13})$$

The value $k_0\delta = n\pi$ still implies $R^+ = -1$ while $k_0\delta = (0.27 + n/2)\pi$ leads to the highest optimal resistance equal to $1.5NS_1/S_w$.

An absorber made of 3 resonator groups has a length of 2δ . For small values of $k_0\delta$, and with $\Re(Z_1^{c,+}/Z_0) = \Gamma$ the lowest reachable resistance, numerically we find that the minimum absorber length for perfect absorption is

$$l_{A,min} = 2\delta = \frac{0.9}{k_0} \sqrt{\frac{\Gamma S_w}{NS_1}}, \quad \text{when } k_0\delta \ll 1. \quad (\text{A.14})$$

A.4. Multiple resonators at the same axial position

With the TMM, point resonators located at the same axial position x_i form a parallel circuit. If the resonators are independent, i.e., if they do no interact, the resonators $i, 1$ to i, N can be represented by a single equivalent resonator of surface impedance $\tilde{Z}_{i,eq}$ given by

$$\frac{1}{\tilde{Z}_{i,eq}} = \sum_{j=1}^N \frac{1}{\tilde{Z}_{i,j}}. \quad (\text{A.15})$$

If the resonators at a given position are identical ($\tilde{Z}_{i,1} = \tilde{Z}_{i,2} = \dots = \tilde{Z}_i$) then the equivalent surface impedance is simply $\tilde{Z}_{i,eq} = \tilde{Z}_i/N$. The group of identical resonators is equivalent to a resonator of lower impedance. This configuration was considered to derive the no-transmission condition, Eq. (10), the no-reflection condition Eq. (12) and the minimal absorber length Eq. (14). Everything goes as if the area S_w of the cross-section of the propagation line was divided by the number N of resonators at the same position, or as if the areas of the resonators connected to the propagation line, S_i , was multiplied by N . Identical resonators can be assembled in groups composed of different number of resonators and form an absorber than can be optimized for perfect absorption [13] as each group has a different equivalent impedance.

As schematized in Fig. A.12, if the resonators at a given position are different, i.e., $\tilde{Z}_{i,1} \neq \tilde{Z}_{i,2} \dots$ the equivalent surface impedance is a combination of their respective impedances.

Combining different resonators at a given axial position is useful to obtain an equivalent impedance having a frequency dependence than could not be realized by a single resonator [12]. For instance, if $\tilde{Z}_{i,1}(f_1) \approx 0$ and $\tilde{Z}_{i,2}(f_2) \approx 0$, then $\tilde{Z}_{i,eq} \approx 0$ at f_1 and f_2 and $T \approx 0$ at f_1 and f_2 which could not be achieved with identical resonators (unless f_2 is a multiple of f_1). Note that to maximize the cancellation of the transmission at a single frequency, the best approach is to combine identical resonators having a zero reactance and the minimal resistance allowed by the considered type of resonator, see Eq. (10). Placing different resonators at the same axial position rather than at different positions does not reduce the number of resonators required for perfect absorption at F frequencies but may help in reducing the length of a broadband absorber.

Appendix B. Mode matching technique

This Appendix presents the MMT equations used in this work. They are adapted from the work of Bi et al. [38], considering cylindrical waveguides, to rectangular cross-section waveguides. Only the specificities of rectangular cross-section waveguides are detailed hereafter.

B.1. Complete orthonormal basis

In the hard walled regions of the waveguide, the modal transverse wave numbers in the y and z directions of order $n \in \mathbb{N}^+$ and $m \in \mathbb{N}^+$, respectively, are

$$k_{yn} = \frac{n\pi}{d_w}, \quad k_{zm} = \frac{m\pi}{h_w}. \tag{B.1}$$

The modal wave number in the direction of propagation x is

$$k_{xmn} = \sqrt{k_0^2 - k_{yn}^2 - k_{zm}^2}, \quad \text{Im}(k_{xmn}) \leq 0. \tag{B.2}$$

A complete orthonormal basis of the hard walled waveguide region is the column vector ψ composed of the ψ_{mn} elements defined as

$$\psi_{mn}(y, z) = \cos(k_{yn}y) \cos(k_{zm}z) \sqrt{\frac{\epsilon_m \epsilon_n}{h_w d_w}}, \tag{B.3}$$

with $\epsilon_0 = 1$, $\epsilon_M = 2 \forall M \neq 0$.

This way, the modal expression of the pressure field is

$$p(x, y, z) = \sum_m \sum_n (P_{mn}^+(x) + P_{mn}^-(x)) \psi_{mn}(y, z), \tag{B.4}$$

$$p(x, y, z) = {}^t \psi (\mathbf{P}^+ + \mathbf{P}^-), \tag{B.5}$$

$$p(x, y, z) = {}^t \psi \mathbf{P}, \tag{B.6}$$

with \mathbf{P} , \mathbf{P}^+ , and \mathbf{P}^- column vectors of same dimension than ψ , being the modal amplitudes of the pressure field, of the forward pressure field and of the backward pressure field, respectively. The transpose operator is noted t .

B.2. Projection of p , $\partial p / \partial x$ and $\Delta_{\perp}(p)$ over the hard walled waveguide modal basis

The projection of p and $\partial p / \partial x$ on the ψ basis read, respectively

$$\int_{y=0}^{d_w} \int_{z=0}^{h_w} p \psi_{mn} dy dz = P_{mn}, \tag{B.7}$$

$$\int_{y=0}^{d_w} \int_{z=0}^{h_w} \frac{\partial p}{\partial z} \psi_{mn} dy dz = P_{mn}'. \tag{B.8}$$

The projection of $\Delta_{\perp}(p)$ with $\Delta_{\perp} = \partial^2 / \partial y^2 + \partial^2 / \partial z^2$, on the ψ basis reads, according to the Green's second identity:

$$\int_{y=0}^{d_w} \int_{z=0}^{h_w} \Delta_{\perp}(p) \psi_{mn} dy dz = \int_y \int_z p \Delta_{\perp}(\psi_{mn}) dy dz + \int_{\Gamma} \psi_{mn} \mathbf{grad}_r(p) - p \mathbf{grad}_r(\psi_{mn}) d\Gamma, \tag{B.9}$$

with Γ the edge of the waveguide at a position x .

As $\Delta_{\perp}(\psi_{mn}) = -(k_{yn}^2 + k_{zm}^2) \psi_{mn}$, then

$$\int_{y=0}^{d_w} \int_{z=0}^{h_w} p \Delta_{\perp}(\psi_{mn}) dy dz = -(k_{yn}^2 + k_{zm}^2) P_{mn}. \tag{B.10}$$

The edges terms are

$$\int_{\Gamma} p \mathbf{grad}_r(\psi_{mn}) d\Gamma = 0, \tag{B.11}$$

and, considering that all the waveguide walls can be lined by a treatment,

$$\int_{\Gamma} \mathbf{grad}_r(p) \psi d\Gamma = -i\omega \rho_0 \mathbf{P} \mathbf{C}(x), \tag{B.12}$$

with

$$\mathbf{C}(x) = \int_{y=0}^{d_w} \left(\frac{1}{Z_s(x, y, 0)} \psi(z=0)^t \psi(z=0) + \frac{1}{Z_s(x, y, h_w)} \psi(z=h_w)^t \psi(z=h_w) \right) dy \tag{B.13}$$

$$+ \int_{z=0}^{h_w} \left(\frac{1}{Z_s(x, 0, z)} \psi(y=0)^t \psi(y=0) + \frac{1}{Z_s(x, d_w, z)} \psi(y=d_w)^t \psi(y=d_w) \right) dz. \tag{B.14}$$

and Z_s the surface impedance at a given waveguide wall location.

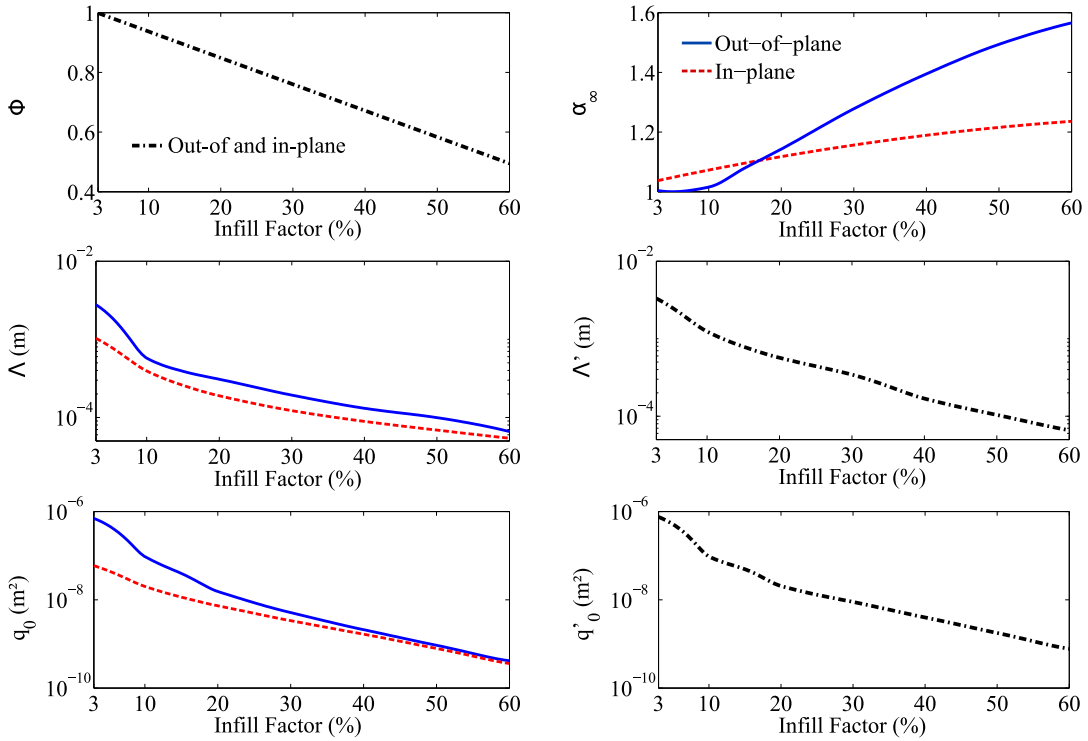


Fig. C.13. Variation of the JCAL parameters of the micro-lattice in function of its Infill Factor (IF) obtained from an inverse characterization process based on impedance tube measurements.

B.3. Modal propagation equation

Then, the pressure modal differential equation in a portion of the waveguide of constant axial surface impedance is

$$\mathbf{P}''(x) + \mathbf{A}(x)\mathbf{P}(x) = \mathbf{0}, \tag{B.15}$$

with \mathbf{A} a piecewise constant tensor along x that reads

$$\mathbf{A}(x) = -\mathbf{L} + \frac{\omega^2 \rho_0}{K_0} \mathbf{I} - i\omega \rho_0 \mathbf{C}(x). \tag{B.16}$$

and \mathbf{L} a diagonal matrix with $k_{yn}^2 + k_{zm}^2$ on the diagonal.

Appendix C. JCAL parameters of the considered micro-lattice

The variation of the porosity, ϕ , the tortuosity, α_∞ , the viscous and thermal characteristic lengths, Λ and Λ' and the viscous and thermal static permeabilities q_0 and q'_0 of the considered micro-lattice in function of IF are presented in Fig. C.13. These variations are obtained through the inverse characterization of several homogeneous samples characterized in an impedance tube [44]. As the micro-lattice is a quasi-isotropic medium, the value of α_∞ , Λ , q_0 depend on the wave propagation direction (in-plane or out-of-plane).

References

- [1] Daniel Potente, General Design Principles for an Automotive Muffler. Busselton, 2005.
- [2] J.-P. Dalmont, E. Portier, Optimisation of anechoic duct termination using line theory, 117, 141–144. <http://dx.doi.org/10.1016/j.apacoust.2016.10.024>.
- [3] A. Merkel, G. Theocharis, O. Richoux, V. Romero-García, V. Pagneux, Control of acoustic absorption in one-dimensional scattering by resonant scatterers, Appl. Phys. Lett. 107 (24) (2015) 244102, <http://dx.doi.org/10.1063/1.4938121>.
- [4] S. Kumar, H.P. Lee, Recent advances in acoustic metamaterials for simultaneous sound attenuation and air ventilation performances, 2020, p. 25.
- [5] N. Jiménez, V. Romero-García, V. Pagneux, J.-P. Groby, Rainbow-trapping absorbers: Broadband, perfect and asymmetric sound absorption by subwavelength panels for transmission problems, Sci. Rep. 7 (1) (2017) 13595, <http://dx.doi.org/10.1038/s41598-017-13706-4>.
- [6] N. Jiménez, W. Huang, V. Romero-García, V. Pagneux, J.-P. Groby, Ultra-thin metamaterial for perfect and quasi-omnidirectional sound absorption, Appl. Phys. Lett. 109 (12) (2016) 121902, <http://dx.doi.org/10.1063/1.4962328>.
- [7] X. Xiang, X. Wu, X. Li, P. Wu, H. He, Q. Mu, S. Wang, Y. Huang, W. Wen, Ultra-open ventilated metamaterial absorbers for sound-silencing applications in environment with free air flows, Extreme Mech. Lett. 39 (2020) 100786, <http://dx.doi.org/10.1016/j.eml.2020.100786>.

- [8] M. Yang, C. Meng, C. Fu, Y. Li, Z. Yang, P. Sheng, Subwavelength total acoustic absorption with degenerate resonators, *Appl. Phys. Lett.* 107 (10) (2015) 104104, <http://dx.doi.org/10.1063/1.4930944>.
- [9] V. Romero-García, N. Jiménez, J.-P. Groby, A. Merkel, V. Tournat, G. Theocharis, O. Richoux, V. Pagneux, Perfect absorption in mirror-symmetric acoustic metascreens, *Phys. Rev. A* 14 (5) (2020) 054055, <http://dx.doi.org/10.1103/PhysRevApplied.14.054055>.
- [10] P. Wei, C. Croënne, S. Tak Chu, J. Li, Symmetrical and anti-symmetrical coherent perfect absorption for acoustic waves, *Appl. Phys. Lett.* 104 (12) (2014) 121902, <http://dx.doi.org/10.1063/1.4869462>.
- [11] H. Long, C. Liu, C. Shao, Y. Cheng, J. Tao, X. Qiu, X. Liu, Tunable and broadband asymmetric sound absorptions with coupling of acoustic bright and dark modes, 479, 115371. <http://dx.doi.org/10.1016/j.jsv.2020.115371>.
- [12] H. Long, Y. Cheng, X. Liu, Asymmetric absorber with multiband and broadband for low-frequency sound, *Appl. Phys. Lett.* (2017) 6.
- [13] H. Long, Y. Cheng, X. Liu, Reconfigurable sound anomalous absorptions in transparent waveguide with modularized multi-order helmholtz resonator, 8 (1) 15678. <http://dx.doi.org/10.1038/s41598-018-34117-z>.
- [14] E.R. Fotsing, A. Dubourg, A. Ross, J. Mardjono, Acoustic properties of periodic micro-structures obtained by additive manufacturing, *Appl. Acoust.* 148 (2019) 322–331, <http://dx.doi.org/10.1016/j.apacoust.2018.12.030>.
- [15] S. Deshmukh, H. Ronge, S. Ramamoorthy, Design of periodic foam structures for acoustic applications: Concept, parametric study and experimental validation, *Mater. Des.* 175 (2019) 107830, <http://dx.doi.org/10.1016/j.matdes.2019.107830>.
- [16] T.G. Zieliński, K.C. Opiela, P. Pawłowski, N. Dauchez, T. Boutin, J. Kennedy, D. Trimble, H. Rice, B. Van Damme, G. Hannema, R. Wróbel, S. Kim, S. Ghaffari Mosanenzadeh, N.X. Fang, J. Yang, B. Briere de La Hosserey, M.C. Hornikx, E. Salze, M.-A. Galland, R. Boonen, A. Carvalho de Sousa, E. Deckers, M. Gaborit, J.-P. Groby, Reproducibility of sound-absorbing periodic porous materials using additive manufacturing technologies: Round robin study, *Addit. Manuf.* 36 (2020) 101564, <http://dx.doi.org/10.1016/j.addma.2020.101564>.
- [17] D.C. Akiwate, M.D. Date, B. Venkatesham, S. Suryakumar, Acoustic properties of additive manufactured narrow tube periodic structures, *Appl. Acoust.* 136 (2018) 123–131, <http://dx.doi.org/10.1016/j.apacoust.2018.02.022>.
- [18] Z. Liu, J. Zhan, M. Fard, J.L. Davy, Acoustic properties of a porous polycarbonate material produced by additive manufacturing, *Mater. Lett.* 181 (2016) 296–299, <http://dx.doi.org/10.1016/j.matlet.2016.06.045>.
- [19] L. Bargaet, V. Romero-García, N. Jiménez, L.M. Garcia-Raffi, V.J. Sánchez-Morcillo, J.-P. Groby, Natural sonic crystal absorber constituted of seagrass (*posidonia oceanica*) fibrous spheres, 11 (1) 711. <http://dx.doi.org/10.1038/s41598-020-79982-9>.
- [20] M.R. Stinson, The propagation of plane sound waves in narrow and wide circular tubes, and generalization to uniform tubes of arbitrary cross-sectional shape, *J. Acoust. Soc. Am.* 89 (2) (1991) 550–558, <http://dx.doi.org/10.1121/1.400379>.
- [21] D. Lafarge, P. Lemarinié, J. Allard, V. Tarnow, Dynamic compressibility of air in porous structures at audible frequencies, *J. Acoust. Soc. Am.* 102 (1997) 1995–2006, <http://dx.doi.org/10.1121/1.419690>.
- [22] J.-F. Allard, N. Atalla, *Propagation of Sound in Porous Media: Modelling Sound Absorbing Materials*, second ed., Wiley, Hoboken, N.J., 2009.
- [23] T. Cavaliéri, J. Boulvert, L. Schwan, G. Gabard, V. Romero-García, J.-P. Groby, M. Escoufflaire, J. Mardjono, Acoustic wave propagation in effective graded fully anisotropic fluid layers, *J. Acoust. Soc. Am.* 146 (5) (2019) 3400–3408, <http://dx.doi.org/10.1121/1.5131653>.
- [24] V. Dubos, A. Kheftabi, D.H. Keefe, C.J. Nederveen, A. Pijnacker, Theory of sound propagation in a duct with a branched tube using modal decomposition, *Acta Acust.* 85 (1999) 18.
- [25] J.-P. Groby, A. Duclos, O. Dazel, L. Boeckx, W. Lauriks, Absorption of a rigid frame porous layer with periodic circular inclusions backed by a periodic grating, *J. Acoust. Soc. Am.* 129 (5) (2011) 3035–3046, <http://dx.doi.org/10.1121/1.3561664>.
- [26] L. Lagarrigue, J.-P. Groby, V. Tournat, O. Dazel, B. Nennig, Acoustic panel.
- [27] T. Cavaliéri, J. Boulvert, V. Romero-García, G. Gabard, M. Escoufflaire, J. Regnard, J.-P. Groby, Rapid additive manufacturing of optimized anisotropic metaporous surfaces for broadband absorption, 129 (11) (2021) 115102. <http://dx.doi.org/10.1063/5.0042563>.
- [28] W. Chen, S. Liu, L. Tong, S. Li, Design of multi-layered porous fibrous metals for optimal sound absorption in the low frequency range, *Theor. Appl. Mech. Lett.* 6 (1) (2016) 42–48, <http://dx.doi.org/10.1016/j.taml.2015.12.002>.
- [29] J. Boulvert, T. Cavaliéri, J. Costa-Baptista, L. Schwan, V. Romero-García, G. Gabard, E.R. Fotsing, A. Ross, J. Mardjono, J.-P. Groby, Optimally graded porous material for broadband perfect absorption of sound, *J. Appl. Phys.* 126 (17) (2019) 175101, <http://dx.doi.org/10.1063/1.5119715>.
- [30] T. Cavaliéri, J. Boulvert, G. Gabard, V. Romero-García, M. Escoufflaire, J. Regnard, J.-P. Groby, Graded and anisotropic porous materials for broadband and angular maximal acoustic absorption, 13 (20) 4605. <http://dx.doi.org/10.3390/ma13204605>.
- [31] B. Howerton, T. Parrott, Validation of an acoustic impedance prediction model for skewed resonators, in: 15th AIAA/CEAS Aeroacoustics Conference (30th AIAA Aeroacoustics Conference), American Institute of Aeronautics and Astronautics, Miami, Florida, 2009, <http://dx.doi.org/10.2514/6.2009-3143>.
- [32] X. Cai, Q. Guo, G. Hu, J. Yang, Ultrathin low-frequency sound absorbing panels based on coplanar spiral tubes or coplanar Helmholtz resonators, *Appl. Phys. Lett.* 105 (12) (2014) 121901, <http://dx.doi.org/10.1063/1.4895617>.
- [33] J. Boulvert, J. Costa-Baptista, T. Cavaliéri, V. Romero-García, G. Gabard, E.R. Fotsing, A. Ross, M. Perna, J. Mardjono, J.-P. Groby, Folded metaporous material for sub-wavelength and broadband perfect sound absorption, *Appl. Phys. Lett.* 117 (25) (2020) 251902, <http://dx.doi.org/10.1063/5.0032809>.
- [34] R. Sugimoto, P. Murray, R.J. Astley, Folded cavity liners for turbofan engine intakes, in: 18th AIAA/CEAS Aeroacoustics Conference (33rd AIAA Aeroacoustics Conference), 2012, p. 2291.
- [35] A.T. Chambers, J.M. Manimala, M.G. Jones, Design and optimization of 3d folded-core acoustic liners for enhanced low-frequency performance, *AIAA J.* 58 (1) (2020) 206–218.
- [36] B. Brouard, D. Lafarge, J.-F. Allard, A general method of modelling sound propagation in layered media, 183 (1) 129–142.
- [37] S.W. Rienstra, *Fundamentals of Duct Acoustics*, 2015, p. 52.
- [38] W. Bi, V. Pagneux, D. Lafarge, Y. Aurégan, Modelling of sound propagation in a non-uniform lined duct using a Multi-Modal Propagation Method, *J. Sound Vib.* 289 (4–5) (2006) 1091–1111, <http://dx.doi.org/10.1016/j.jsv.2005.03.021>.
- [39] J. Guo, X. Zhang, Y. Fang, Broadband forbidden transmission by multiple CPA-based detuned Helmholtz resonators, in: ICSV26, Montréal, 2019, p. 8.
- [40] J.A. Nelder, R. Mead, A simplex method for function minimization, *Comput. J.* 7 (4) (1965) 308–313, <http://dx.doi.org/10.1093/comjnl/7.4.308>.
- [41] J. Guo, Reflected Wave Manipulation and Noise Attenuation Based on Inhomogeneous-Distributed Resonators (Ph.D), The Hong Kong University of Science and Technology, Clear Water Bay, Kowloon, Hong Kong, 2019, 991012763468803412, <http://dx.doi.org/10.14711/thesis-991012763468803412>.
- [42] M.E. D'Elia, T. Humbert, Y. Aurégan, Effect of flow on an array of Helmholtz resonators: Is Kevlar a magic layer? *J. Acoust. Soc. Am.* 148 (6) (2020) 3392–3396, <http://dx.doi.org/10.1121/10.0002642>.
- [43] J. Boulvert, T. Humbert, V. Romero-García, G. Gabard, E.R. Fotsing, A. Ross, J. Mardjono, J.-P. Groby, Asymmetric metaporous treatment: Optimization for perfect sound absorption, 3d printing, and characterization with air flow, in: 2021 Fifteenth International Congress on Artificial Materials for Novel Wave Phenomena (Metamaterials), IEEE, pp. 065–067. <http://dx.doi.org/10.1109/Metamaterials52332.2021.9577098>.
- [44] J. Boulvert, J. Costa-Baptista, T. Cavaliéri, M. Perna, E.R. Fotsing, V. Romero-García, G. Gabard, A. Ross, J. Mardjono, J.-P. Groby, Acoustic modeling of micro-lattices obtained by additive manufacturing, *Appl. Acoust.* 164 (2020) 107244, <http://dx.doi.org/10.1016/j.apacoust.2020.107244>.